ANALYSIS AND DESIGN OF CYLINDRICALLY CONFORMAL MICROSTRIP ANTENNAS

A THESIS SUBMITTED TO
THE GRADUATE SCHOOL OF NATURAL AND APPLIED SCIENCES
OF
MIDDLE EAST TECHNICAL UNIVERSITY

BY

ALİ ÖZGÜR TAŞOĞLU

IN PARTIAL FULFILLMENT OF THE REQUIREMENTS
FOR
THE DEGREE OF MASTER OF SCIENCE
IN
ELECTRICAL AND ELECTRONICS ENGINEERING

JULY 2011

Approval of the thesis:

ANALYSIS AND DESIGN OF CYLINDRICALLY CONFORMAL MICROSTRIP ANTENNAS

submitted by **ALİ ÖZGÜR TAŞOĞLU** in partial fulfillment of the requirements for the degree of **Master of Science in Electrical and Electronics Engineering Department, Middle East Technical University** by,

Prof. Dr. Canan Özgen _____
Dean, Graduate School of **Natural and Applied Sciences**

Prof. Dr. İsmet Erkmen _____
Head of Department, **Electrical and Electronics Engineering**

Prof. Dr. Gülbin Dural _____
Supervisor, **Electrical and Electronics Engineering Dept., METU**

Examining Committee Members:

Prof. Dr. S. Sencer Koç _____
Electrical and Electronics Engineering Dept., METU

Prof. Dr. Gülbin Dural _____
Electrical and Electronics Engineering Dept., METU

Assoc. Prof. Dr. Lale Alatan _____
Electrical and Electronics Engineering Dept., METU

Assoc. Prof. Dr. Şimsek Demir _____
Electrical and Electronics Eng. Dept., METU

Dr. Özlem ŞEN _____
TÜBİTAK Space Tech. Research Ins.

Date: July 12, 2011

I hereby declare that all information in this document has been obtained and presented in accordance with academic rules and ethical conduct. I also declare that, as required by these rules and conduct, I have fully cited and referenced all material and results that are not original to this work.

Name, Last name: Ali Özgür Taşoğlu

Signature:

ABSTRACT

ANALYSIS AND DESIGN OF CYLINDRICALLY CONFORMAL MICROSTRIP ANTENNAS

Taşoğlu, Ali Özgür

M.Sc., Department of Electrical and Electronics Engineering

Supervisor: Prof. Dr. Gülbin Dural

July 2011, 85 pages

Cylindrically conformal microstrip antennas are investigated. Two different structures, namely proximity coupled and E-shaped microstrip antennas are analyzed and information about the design parameters is obtained by means of parametric study. With these structures, cylindrical arrays, having omnidirectional radiation in the circumferential plane of the cylinder, are designed. Proximity coupled cylindrical arrays operate in the 2.3-2.4 GHz aeronautical telemetry band with approximately 4% bandwidth. On the other hand, more than 30% bandwidth is obtained by E-Shaped cylindrical array antenna structure, which also includes the commercial telemetry band. In order to verify the simulation method, a fabricated antenna in literature is simulated and acceptable agreement with simulation and fabrication results obtained.

Keywords: Microstrip Patch, Cylindrical Antenna, E-shaped Patch Antenna, Proximity Coupled Patch, Conformal Antenna, Broadband Antenna

ÖZ

SİLİNDİRİK UYUMLU MİKROŞERİT ANTENLERİN TASARIMI VE ANALİZİ

Taşoğlu, Ali Özgür

Yüksek Lisans, Elektrik ve Elektronik Mühendisliği Bölümü

Tez Yöneticisi : Prof. Dr. Gülbin Dural

Temmuz 2011, 85 sayfa

Silindirik uyumlu mikroşerit antenler araştırılmıştır. İki değişik yapı, yakınlık eşleşmeli ve E-şekilli mikroşerit antenler, analiz edilmiş ve parametrik çalışma ile tasarım parametreleri hakkında bilgi edinilmiştir. Bu yapılarla, silindirin çevresel düzleminde çok yönlü yayılıma sahip olan silindirik anten dizileri tasarlanmıştır. Yakınlık eşleşmeli silindirik anten dizileri 2.3-2.4 GHz telemetre bandında yaklaşık olarak %4 band genişliğinde çalışmaktadır. Diğer yandan, E-şekilli silindirik anten dizisi yapısı ile ticari telemetre bandını da içeren %30'dan daha fazla bant genişliği elde edilmiştir, Benzetim metodunu doğrulamak için, literatürdeki üretilmiş bir anten yapısı tekrar edilmiş ve benzetim sonuçları ile üretim test sonuçları arasında kabul edilebilir bir uyum gözlemlenmiştir.

Anahtar kelimeler: Mikroşerit Yama, Silindirik Anten, E-şekilli Anten, Yakınlık Eşleşmeli Yama, Geniş Bantlı Anten

To My Dear Family

ACKNOWLEDGEMENTS

I would like to thank Prof. Dr. Gülbin Dural for her supervision, encouragement and support throughout the research. Her advices and opinions helped me as a young researcher and I am very glad to have a chance to work with her.

I would like to thank Prof. Dr. S. Sencer Koç, Assoc. Prof. Dr. Lale Alatan, Assoc. Prof. Dr. Şimsek Demir and Dr. Özlem Şen for participating in my committee and sharing their ideas.

I would like to thank my friends Serhat Acar, Erkan Abbasioğlu, Ertan Yazıcı and Kemal Sakal for their endless encouragement, help and patience during all parts of this study. Without their support, this work would have never been accomplished.

Lastly, I would like to express my deepest gratitude to my family for giving courage and strength in completing this thesis. They have always been a perfect supporter in every parts of this work.

TABLE OF CONTENTS

LIST OF TABLES

TABLES

LIST OF FIGURES

FIGURES

CHAPTER 1

INTRODUCTION

Deschamps introduced Microstrip antennas in 1953 [1]. However the first practical antennas were fabricated during 1970s by Munson [2] and Howell [3]. Since then extensive research has been done on microstrip antennas and numerous configurations have been designed.

A microstrip antenna is made up of a radiating patch on one side of a dielectric and a ground plane on the other side. The patch can have any shape but regular shapes are preferred to simplify the analysis and predict the performance of the antenna [4]. The radiation is caused by the fringe fields between the patch and the ground plane of the antenna. The fringe field, in other words the radiation, is improved by reducing the value of the dielectric constant or enlarging the substrate thickness [4].

Microstrip antennas are appropriate for miscellaneous applications. Some of these applications are given in Table 1-1 [5].

Table 1-1 Typical applications of microstrip antennas [5]

System	**Application**
Aircraft and ship antennas	Communication and navigation, altimeters, blind landing systems
Missiles	Radar, proximity fuses, and telemetry
Satellite communications	Domestic direct broadcast TV, vehicle-based antennas, communication
Mobile Radio	Pagers and hand telephones, man pack systems, mobile vehicle
Remote Sensing	Large lightweight apertures
Biomedical	Applicators in microwave hyperthermia
Others	Intruder alarms, personal communication, and so forth

The advantages of microstrip antennas can be summarized as [5].

- They have low weight, thin profile and small volume
- They can be made conformal
- They have low fabrication cost
- Both linear and circular polarization is possible
- They make dual and triple band applications possible
- They can be integrated with Microwave Integrated Circuits easily

However, most of the microstrip antennas suffer from the following disadvantages [5].

- They have narrow bandwidth
- They have lower gain
- They have low power handling capability

Since microstrip antennas have numerous advantages and are suitable for wide range of applications, research has been conducted to minimize the effects of above limitations. The bandwidth, which is the major limiting factor, can be enhanced by means of broadbanding techniques, which will be discussed in Chapter 2. Also, lower gain and power handling capability can be dealt with using an array structure.

For airborne applications, antenna requirement are very strict. The antenna needs to be conformal to the mounting surface, have low profile and weight. Microstrip antennas are a very strong candidate for these applications since they fulfill most of these requirements. Generally, an omnidirectional radiation is used for data-link, telecommand, guidance, control and telemetry purposes. This type of radiation is obtained by wrapping a microstrip patch array around a cylinder [6].

The objective of this thesis is to investigate cylindrically conformal microstrip antennas used in airborne systems. For that purpose, two different antenna structures, namely proximity coupled and E-shaped, are analyzed and design parameters for both structures are studied. In addition, two antenna arrays, having an omnidirectional radiation in the circumferential plane of the cylinder, are designed for each structure. All arrays include the 2.3-2.4 GHz commercial telemetry band and have a minimum of 50 MHz bandwidth.

In Chapter 2, analysis methods of microstrip antennas are presented. Cylindrically conformal microstrip antennas are analyzed and differences between these structures and planar structures are given. In addition, the commonly used broadbanding techniques are discussed in this chapter.

In Chapter 3, parametric study of a proximity coupled cylindrically conformal microstrip antenna by means of a simulation tool is performed. Design parameters of the antenna are investigated and two different cylindrical arrays are realized.

Chapter 4 focuses on a compact broadband structure, namely E-shaped conformal microstrip antenna. This antenna is analyzed parametrically by a simulation program in order to gain information about the design parameters and two different cylindrical arrays are designed. Finally, a fabricated compact broadband antenna structure is simulated and it is observed if the simulation results match the experimental results.

Chapter 5 presents the conclusion and future work which could be performed in the subject of the thesis.

CHAPTER 2

MICROSTRIP ANTENNAS

2.1 Analysis Methods of Microstrip Antennas

There are many methods in the literature to analyze microstrip antennas. Transmission line model, cavity model and full wave analysis techniques are the mostly used methods among these [7]. Transmission line and cavity model give good physical insight about the antenna and can be used in initial design stage. However, to estimate the antenna performance more accurately and reliably, full wave analysis methods are usually preferred. A probe fed rectangular microstrip antenna geometry is given in Figure 2-1.

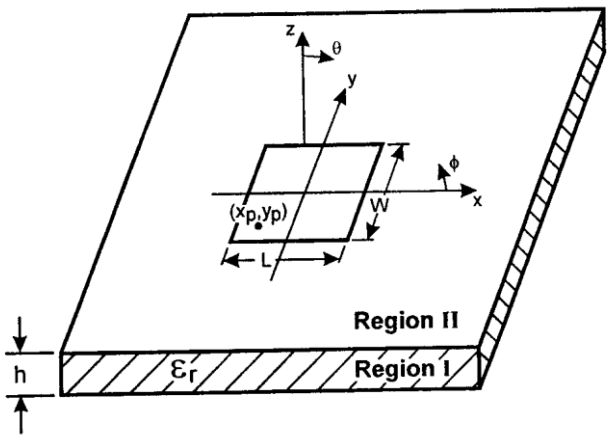

Figure 2-1 Geometry of a coaxially fed rectangular microstrip antenna [4]

Microstrip antennas have physical shape derived from microstrip transmission lines and these antennas can be modeled as sections of transmission lines [4]. Therefore, transmission line model can be utilized to predict the design parameters of the antenna. Due to finite dimensions of the patch, the fields undergo fringing as shown in Figure 2-2. The amount of fringing is a function of substrate height, substrate permittivity and patch width. Because of the fringing fields, the effective length of the patch appears greater than its physical size [7]. Fringing fields are represented by adding ΔL on each side along the length as shown in Figure 2-2.

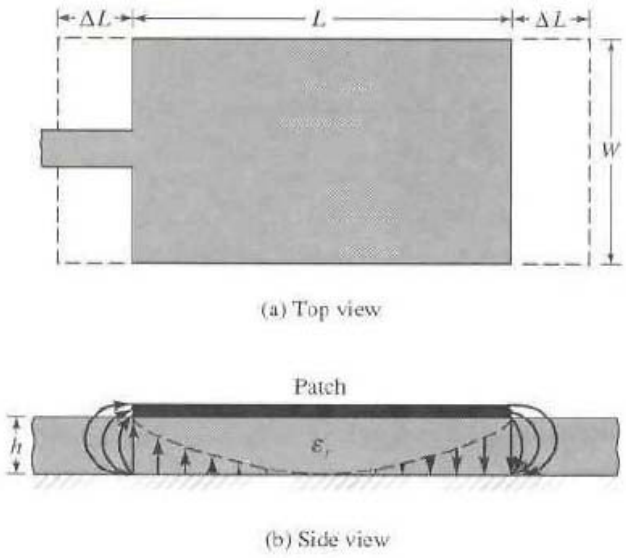

Figure 2-2 Fringe fields of rectangular microstrip antenna [7]

The most popular approximation for the extension ΔL is given in [8] as:

$$\frac{\Delta L}{h} = 0.412 \frac{\left(\varepsilon_{eff} + 0.3\right)\left(\frac{W}{h} + 0.264\right)}{\left(\varepsilon_{eff} - 0.258\right)\left(\frac{W}{h} + 0.8\right)} \tag{2-1}$$

The effective length of the patch becomes

$$L_{eff} = L + 2\Delta L \tag{2-2}$$

The effective dielectric constant ε_{eff} can be calculated as [9].

$$\varepsilon_{eff} = \frac{\varepsilon_r + 1}{2} + \frac{\varepsilon_r + 1}{2}\left[1 + 10\frac{h}{W}\right]^{-1/2} \tag{2-3}$$

The resonant frequency of the antenna is expressed as

$$f_r = \frac{c}{2(L + 2\Delta L)\sqrt{\varepsilon_{eff}}} \tag{2-4}$$

where c is the speed of light.

Microstrip antennas are termed as narrowband resonant lossy cavities. For that reason, the cavity model [10] is also a very good approximation for analyzing microstrip antennas. This technique is very useful in having an insight about the radiation mechanism of the antenna. The model is based on the following assumptions [10].

a. Due to the close proximity between the ground plane and microstrip antenna, E has only z-component and H has only xy-components in the region bounded by the microstrip and the ground plane.

b. The fields in the above mentioned region do not vary with the z coordinate for all frequencies of interest.

c. The electric current in the microstrip has no component normal to the edge, which implies the tangential component of the H is negligible along the edge.

Accordingly, the region between the patch and the ground plane can be regarded as a cavity bounded by magnetic walls along the edge and electric walls from top and bottom. By assuming that the field structure in the microstrip antenna is the same as that in the cavity, the input impedance, the radiation pattern and the total radiated power can be computed for any feed point location [10].

For the geometry of Figure 2-1 the field that satisfies the boundary conditions is of the form:

$$E_z = A_{mn} \cos(\frac{mx\pi}{L}) \cos(\frac{ny\pi}{W}) \tag{2-5}$$

where A_{mn} is the amplitude coefficient of the corresponding TM_{mn} mode. The magnetic current density on the magnetic walls of the patch can be expressed as [10].

$$M = 2\hat{n} \times \hat{z} E_z \tag{2-6}$$

where $\hat{n}$ is the outward normal to the magnetic walls. The electric vector potential of M is as given below [10].

$$F(r) = \varepsilon_0 \int_C \frac{M(r')}{4\pi \mid r - r' \mid} e^{-k_0 \mid r - r' \mid} dl(r') \tag{2-7}$$

The far field at r is [10].

$$E_\theta = \eta H_\phi = jk_0 F_\phi = jk_0 (-F_x \sin\phi + F_y \cos\phi) \tag{2-8}$$

$$E_\phi = -\eta H_\theta = -jk_0 F_\theta = -jk_0 (F_x \cos\theta \cos\phi + F_y \cos\theta \sin\phi) \tag{2-9}$$

The total radiated power is

$$P_r = \mathrm{Re} \int_0^{\pi/2} \int_0^{2\pi} (E_\theta H_\phi^* - E_\phi H_\theta^*) r^2 \sin\theta d\phi d\theta \qquad (2\text{-}10)$$

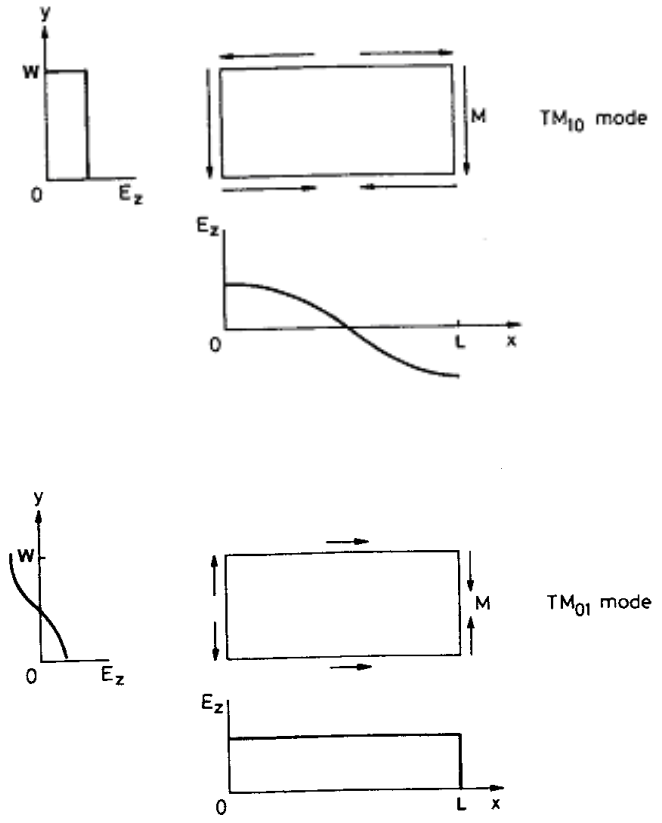

Figure 2-3 Electric field and magnetic surface current densities for the TM_{10} and TM_{01} modes of the Patch Antenna [4]

The electric field and surface magnetic current densities for TM_{10} and TM_{01} modes are given in Figure 2-3. For the TM_{10} mode, magnetic currents along W cancel each other while the ones along L add up. For that reason W is known as "radiating edge" whereas L is known as "non-radiating edge" for TM_{10} mode [11].

If the feed location of the patch is along the W/2 line, TM_{01} is not excited and the antenna will have linear polarization in x-direction. The input impedance of the TM_{10} mode can be simply adjusted by changing the location of the feed along the length of the patch, L.

For the analysis of complex microstrip antenna geometries, full wave methods are more commonly used to predict the antenna performance more accurately. One of the popular numerical methods used is Method of Moments. In this method, the unknown partial differential equation or integral equation in the solution of an electromagnetic problem is approximated by a linear combination of known functions. These known functions are called basis or expansion functions and coefficients are selected so as to make the approximation reasonably accurate. Then the coefficients of the basis functions are solved with the help of weighting functions, which also yields the solution of the electromagnetic problem [7], [12].

The electromagnetic simulator used in this thesis is CST MICROWAVE STUDIO®, which uses Finite Integration Technique (FIT) [13]. A universal spatial discretization scheme is provided in this numerical method which is applicable to various electromagnetic problems in time or frequency domain. In FIT, the integral form of Maxwell's equations is discritized rather than their differential forms. To solve these equations numerically, a finite calculation domain must be defined, which encloses the considered application problem. A suitable mesh system splits this domain up into grid cells [43].

In addition to the primary mesh, a dual mesh is formed orthogonally to the primary mesh by CST. On these two orthogonal grid cells, the spatial discretization of Maxwell's equations is done. Referring to the Figure 2-4, the

electric grid voltages e and magnetic facet fluxes b are allocated on the primary grid, G. Additionally, the dielectric facet fluxes d and the magnetic grid voltages h are defined on the dual grid, $\tilde{G}$ [43].

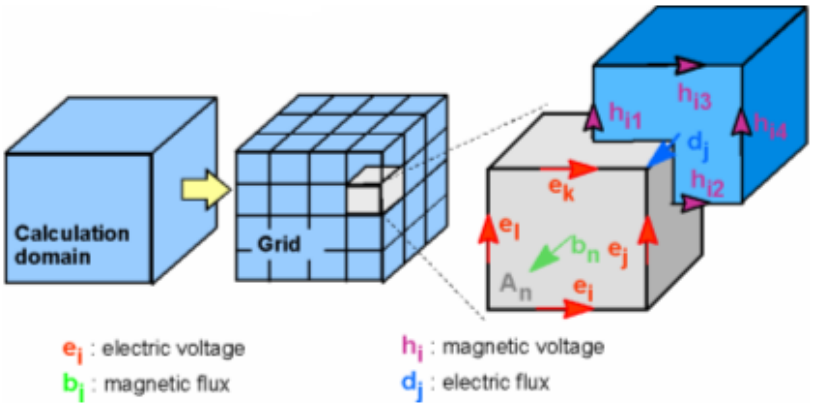

Figure 2-4 Mesh generation in CST [43]

The formulation of Maxwell's equations for each cell facet is shown in the following. Regarding the Faraday's Law, the closed integral on the left hand side of the equation given in Figure 2-5 is represented by the addition of four grid voltages. As a result, time derivative of the magnetic flux that is defined on the enclosed primary cell facet represents the equation's left side as given in Figure 2-5 [43].

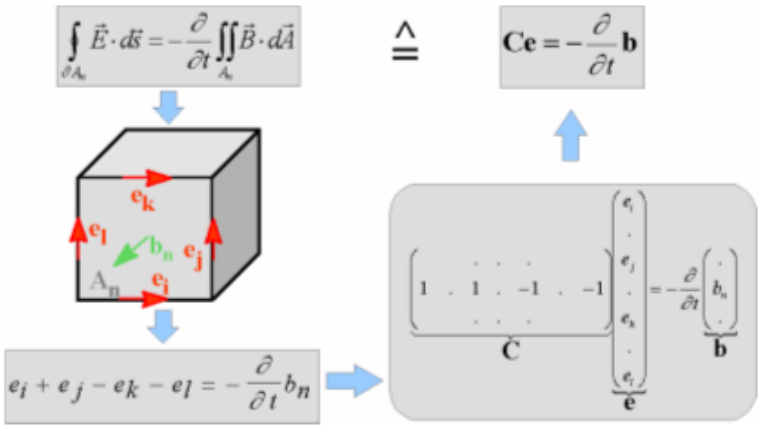

Figure 2-5 Discretization of Maxwell's Equations in CST [43]

Applying the method to all cell facets summarizes the calculation rule in a matrix formulation. In this formulation, the topological matrix C is introduced as the discrete equivalent of the analytical curl operator. The dual discrete curl operator $\tilde{C}$ is introduced when this scheme is applied to Ampere's law. In the same manner, the discretization of the remaining two divergence equations introduces discrete divergence operators S and $\tilde{S}$ for the primary and dual grids, respectively. These discrete matrix operators are made up of elements 0, 1, and -1, which represent only topological information. Finally, the complete discritized set of Maxwell's Grid Equations (MGEs) are obtained [43].

$$Ce = -\frac{d}{dt}b \qquad \tilde{C}h = -\frac{d}{dt}d + j \tag{2-11}$$

$$\tilde{S}d = q \qquad Sb = 0 \tag{2-12}$$

A very useful feature of the FIT is that the important properties of the continuous gradient, curl and divergence operators are still valid in grid space [43].

$$\tilde{S}C = \tilde{S}\tilde{C} = 0 \quad \Leftrightarrow \quad div\ curl = 0 \tag{2-13}$$

$$C\tilde{S}^T = \tilde{C}S^T = 0 \quad \Leftrightarrow \quad curl\ \ grad = 0 \tag{2-14}$$

Finally, the missing material relations are summarized in the matrices given below:

$$\vec{D} = \varepsilon\vec{E} \qquad d = M_\varepsilon e \tag{2-15}$$

$$\vec{B} = \mu\vec{H} \quad \Rightarrow \quad b = M_\mu h \tag{2-16}$$

$$\vec{J} = \sigma\vec{E} + \vec{J}_S \qquad j = M_\sigma e + j_s \tag{2-17}$$

At the end, all matrix equations are found and the electromagnetic field problems can be solved on the discrete grid space. FIT can be applied to more general mesh types like topologically irregular grids and tetrahedral grids as well [43].

2.2 Cylindrically Conformal Microstrip Antennas

A conformal antenna is an antenna that conforms to a prescribed shape. This shape can be a part of an airplane, a missile or other vehicle [14]. These antennas can be used to hide their presence; to save space; or to avoid changing the aerodynamic performance of the vehicle they are mounted on [15]. Microstrip antennas can be conformal which is regarded as one of the major advantages of these structures [16]. The radius of curvature affects the performance of the antenna and this affect has to be analyzed to simplify the design process of the antenna. A microstrip antenna mounted on a cylindrical surface is analyzed in [16] and [17] by using cavity model. Full wave analysis of cylindrical-rectangular microstrip antennas is performed in [15], [18] and [19].

For a rectangular microstrip antenna mounted on a cylindrical surface, it is observed in [14]-[17] that the input impedance and resonant frequency is affected slightly by the radius of curvature for both axial and circumferential polarizations if the height of the dielectric layer is not comparable with the wavelength.

A microstrip patch antenna with L= 44.40 mm and W=66.60 mm is positioned separately on a cylinder as it is shown in Figure 2-6 to have axial and circumferential polarizations. The height of the dielectric layer is 2.3 mm and

relative dielectric constant, ε_r is 2.85 with a loss tangent, $\tan\delta_\varepsilon$, of 0.0073. This configuration yields a resonant frequency at 2.1 GHz and the probe position is adjusted to have 50 Ω input impedance [14].

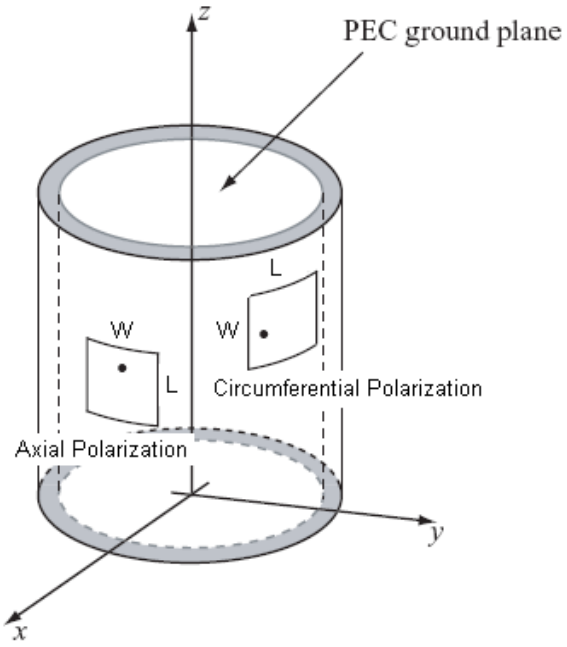

Figure 2-6 Geometry of cylindrical-rectangular microstrip patch antenna (Modified from [14])

Radius of the cylinder is varied between 2λ and 10λ and effect of curvature on input impedance for axial and circumferential polarizations is illustrated in Figure 2-7 and Figure 2-8, respectively. It can be understood from these figures that for axial polarization the input impedance is almost not affected by the curvature. However, for the circumferential polarization, input impedance locus is shifted slightly [14]. In light of these observations, it can be concluded that resonant frequency of the cylindrical patch is nearly same with its planar configuration.

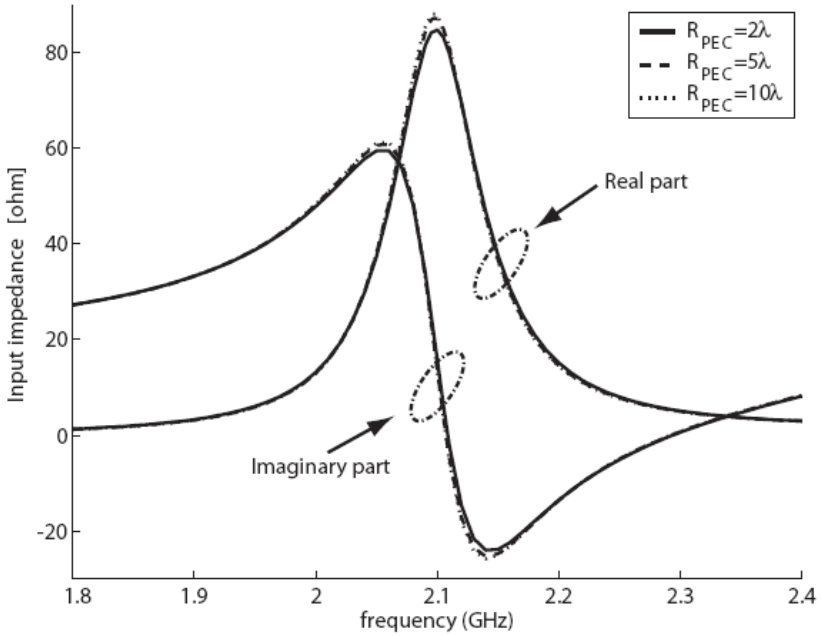

Figure 2-7 The input impedance of a axially polarized patch antenna mounted on a circular cylinder versus radius [14]

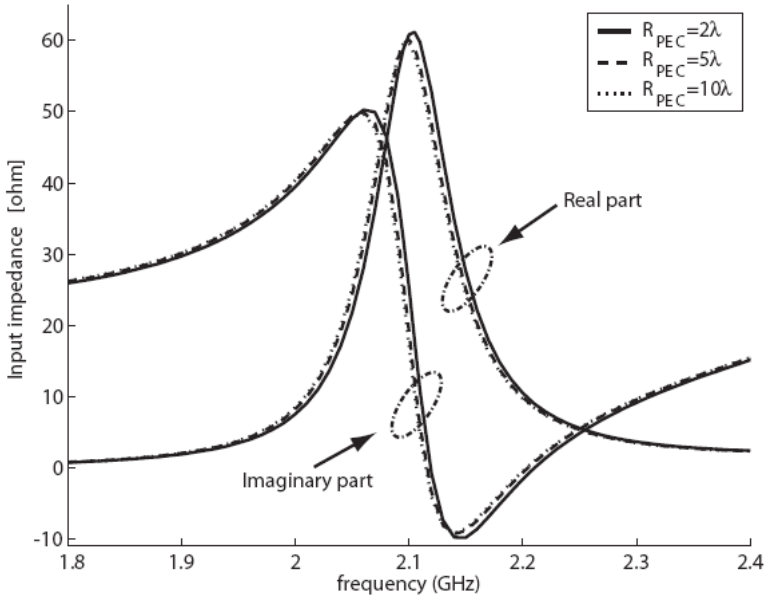

Figure 2-8 The input impedance of a circumferentially polarized patch antenna mounted on a circular cylinder versus radius [14]

It is shown in [14] and [16] that for both axial and circumferential polarizations, only minor changes are observed in the main lobe of the radiated field with different radius of curvature. The deviation from flat patch is higher for larger ε_r. It is also shown that back radiation is increased when radius of curvature of the antenna is decreased. Compared to axial polarization, back radiation is higher for circumferential polarization [16].

For axial polarization, bandwidth increases as curvature increases. On the other hand, bandwidth can either decrease or increase depending on the value of relative dielectric constant, ε_r for circumferential polarization [16].

2.3 Broadbanding of Microstrip Antennas

Microstrip antennas have narrow bandwidth which is the major limit for their widespread use. The bandwidth of these antennas enhances as the substrate thickness increase or the value of dielectric constant reduces. However, there is a practical limit of increase in substrate thickness above which surface wave propagation causes degradation in antenna performance. Also, when substrate thickness increases, the probe inductance increases and matching of the antenna to the feed line becomes challenging. Increasing the bandwidth of microstrip antennas by various methods has been the major goal of researchers in this field and broad bandwidth up to 70% has been achieved. Various broadband microstrip antenna configurations are realized and the commonly used ones are given in the following sections [5].

2.3.1 Multiresonator Planar Broadband Microstrip Antennas

If a parasitic patch is located near a fed patch as in Figure 2-9, it gets excited by electromagnetic coupling between the patches. When these two patches have close resonant frequencies, a broad bandwidth can be acquired [5].

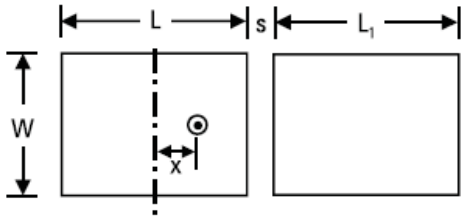

Figure 2-9 One edge gap-coupled microstrip antenna [5]

The coupling is also achieved directly by using microstrip lines as illustrated in Figure 2-10, which is known as direct coupling.

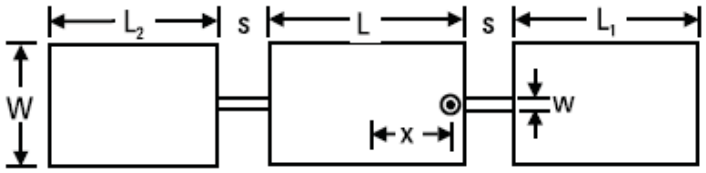

Figure 2-10 Two edge directly-coupled microstrip antenna [5]

The coupling can be made along the radiating, W or non-radiating edge, L. In addition, four edge coupled structure can be realized to increase bandwidth further. For this structure, both radiating and non-radiating edge coupling is achieved. Four edge gap-coupled patch antenna is shown in Figure 2-11. There is no doubt that four edge directly-coupled microstrip antenna is same with the one in Figure 2-11 except with the coupling microstrip lines [5].

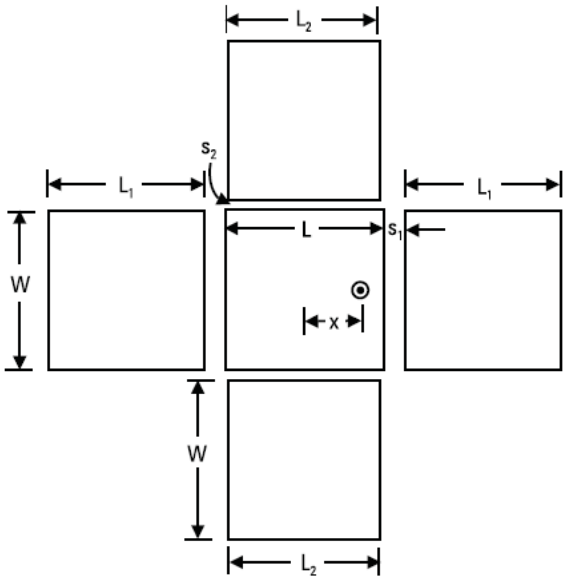

Figure 2-11 Four edge gap-coupled microstrip antenna [5]

By using planar multiresonator configuration, the bandwidth improves without increasing the thickness of the antenna. However, these structures are not suitable for use as an array element since their planar size is large. In addition, the radiation pattern of these antennas varies over the impedance bandwidth, which is not desired for array elements [5].

2.3.2 Multilayer Broadband Microstrip Antennas

In this technique two or more patches on different layers of dielectric substrate are stacked on each other. Based on the coupling mechanism, these structures are classified as electromagnetically coupled or aperture coupled microstrip antennas [5], [20].

An electromagnetically coupled patch antenna structure is given in Figure 2-12. The bottom patch is excited through a coaxial probe while the top patch is excited by electromagnetic coupling with the bottom patch. The neighboring

resonant frequencies of the two patches produce broad bandwidth. More than two patches can be used to further enhance the bandwidth. Alternatively, the two dielectric layers can be spaced by an air gap for the purpose of increasing the bandwidth [20], [21].

Figure 2-12 Electromagnetically coupled microstrip antenna [5]

Electromagnetic coupling can also be used to excite the patch on the upper layer by a feed line on the bottom layer as shown in Figure 2-13. This configuration has the advantage that feed line is closer to the ground resulting in the reduction of the feed radiation. Also, the match between the line and the patch can be simply achieved by adjusting the patch width or changing the feed line length relative to the central point of the patch. Lastly, there is no direct connection between the patch and the feed which makes the production of the antenna easy [22], [23]. Analysis and design rules of proximity coupled microstrip antenna are presented in [22]-[26].

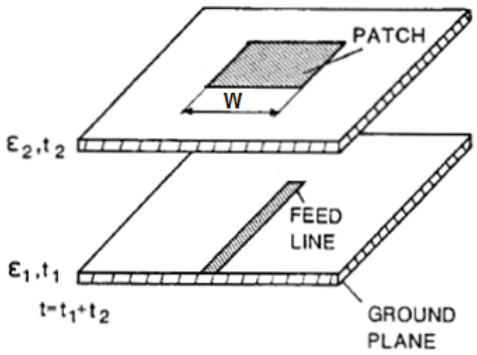

Figure 2-13 Proximity coupled microstrip antenna (Modified from [22])

In aperture coupled microstrip antenna, coupling from the feed line to the patch is accomplished by means of an aperture as shown in Figure 2-14. This antenna is first proposed in 1985 and it consists of two layers of dielectric separated by a ground plane [27]. Several techniques [27] - [31] have been used to analyze the structure and they give good design estimates.

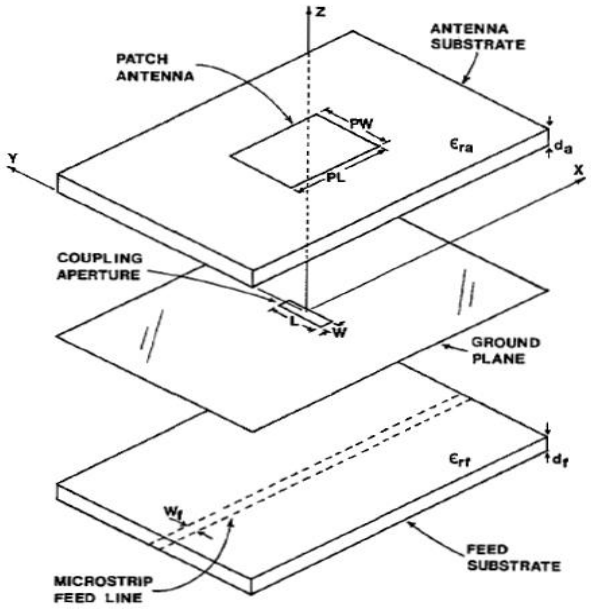

Figure 2-14 Aperture coupled microstrip patch antenna [28]

There are some advantages of using aperture coupled structure. First of all, feed line and the patch are separated by ground plane that means the feed radiation does not disturb the main radiation of the antenna. Furthermore, matching of the antenna to the feed line is simply achieved by changing the physical parameters of the aperture. Lastly, since there is no direct connection between the antenna and feed line, problems related to the large probe self reactances or wide microstrip lines are avoided. The disadvantages of the structure include difficulty in production and relatively high thickness to have reasonably wide bandwidth [27], [29].

Multilayered structures are suitable to be used as array elements since the planar size of the antenna remains the same and the radiation pattern is stable over the broad bandwidth. However, for conformal array applications where a thin profile is desired, multilayer broadband antennas may not be a good choice.

2.3.3 Compact Broadband Microstrip Antennas

In compact broadband structures, wide bandwidth is accomplished neither by increasing the planar size nor the height of the antenna. In these structures a slot is cut inside or along the periphery of the patch for the purpose of increasing the bandwidth. The wide bandwidth of these antennas is the result of neighboring resonant frequencies of the slot and the patch. One of these types of antennas is the probe fed U-slot rectangular patch antenna. This structure is first proposed by Huynh and Lee [32] in 1995 and is shown in Figure 2-15.

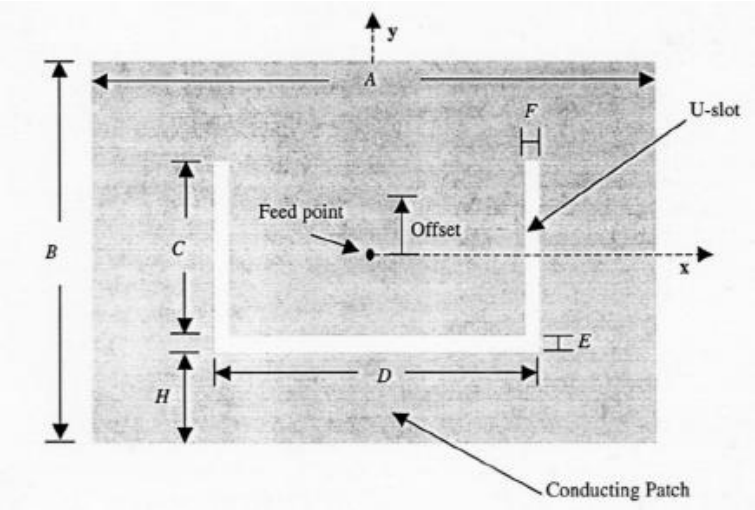

Figure 2-15 Probe fed U-slot microstrip patch antenna [38]

With the addition of the slot, the U-slot patch antenna shows mainly two resonant frequencies. The lower resonant frequency of the U-slot antenna is due to the resonant frequency of the patch. However, this frequency is lower than that of the normal patch since current paths are disturbed by the slot. The higher resonant frequency of the U-slot rectangular patch antenna is the result of the U-slot. The lower and higher resonant frequencies together are responsible for the broadband characteristics [32]-[38]. Approximate design formulas for the geometry are provided in [37] and [38] which are very useful for the initial design.

Another compact broadband structure is probe fed E-shaped rectangular patch antenna. The principle of operation, radiation characteristics and bandwidth of this antenna is similar to those reported for U-slot patch antenna. In contrast to U-slot patch antenna, the lower resonant frequency of the E-shaped antenna is determined by the slots whereas the higher resonant frequency is characterized by the resonant frequency of the patch. Moreover, this antenna has a simpler design than U-slot patch antenna [39]-[42].

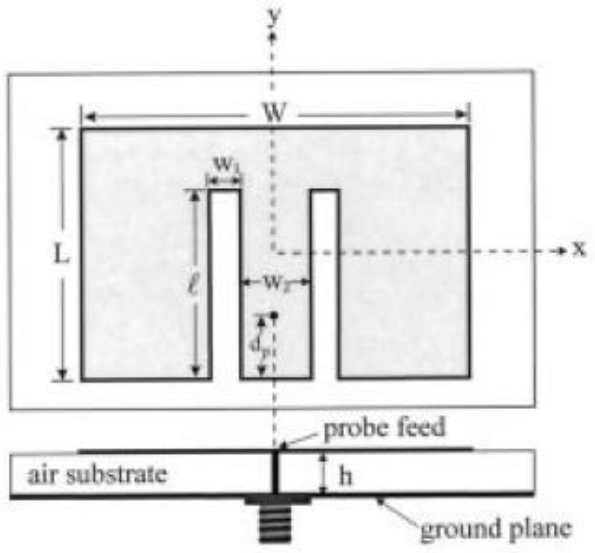

Figure 2-16 Probe fed E-shaped rectangular patch antenna [40]

Both U-slot and E-shaped antennas have good co-polarization radiation characteristics in the broad bandwidth. However, these two antennas have higher cross-polarization in the H-plane compared to the regularly shaped patch antenna. This higher cross-polarization value is caused by the leaky behavior of the slots but acceptable for most of the communication applications [32]-[42].

In compact broadband patch antennas, the substrate needs to be electrically thick to have broadband characteristics. However, this thickness is much smaller than the thickness of the multilayer configuration that has the same bandwidth. For that reason these structures are very advantageous in terms of the size when compared to other broadband patch antennas.

Other slot shapes can be cut on the patch to increase the bandwidth but above mentioned methods are simpler in analysis and production. The main idea behind the slotted patches is that; when thick substrate is used, it causes large probe inductance which can not be compensated by changing the feed location of the antenna. By incorporating a slot, a capacitive reactance is created which compensates the large probe inductive reactance and broadband is achieved [32]-[42].

CHAPTER 3

ANALYSIS AND DESIGN OF PROXIMITY COUPLED CYLINDRICALLY CONFORMAL MICROSTRIP ANTENNA ARRAYS

In section 3.1 of this chapter, parametric studies of a proximity coupled cylindrically conformal microstrip antenna are carried out. Then, in section 3.2, proximity coupled cylindrically conformal microstrip antennas are used to analyze and design cylindrically conformal microstrip antenna arrays. For the cases investigated in this section, resonance frequency of 2.35 GHz is used.

The simulations are performed in CST MICROWAVE STUDIO®, which is one of the well known and reliable simulation tools. The program meshes the 3-D structures automatically and it is clear that the accuracy of the results increases when meshes are refined. For that purpose, the program uses adaptive meshing in which the number of meshes is increased adaptively until the convergence criterion is reached. By this way, the simulation time and memory required for the computation is minimized. Alternatively, the meshing can be done manually by the user.

3.1 Parametric Analysis of Proximity Coupled Cylindrically Conformal Microstrip Antenna Element

A proximity coupled microstrip antenna which is conformal to a cylindrical surface is studied parametrically to obtain information about the design parameters. Each time one variable is changed while keeping the others constant. In conformal antenna applications flexible substrates need to be used in order to allow bending. For that reason Arlon IsoClad 933 substrate is chosen which can be bent easily and is available in the material library of CST. The material is used with a standard thickness of 0.062 inch (1.575mm) and electrodeposited copper of 2 oz (0.07mm). The width of the feed line is chosen as 4.2 mm to have characteristic impedance of 50 Ω. Feed line is located below the W/2 line; therefore the antenna is axially polarized. Design parameters of the antenna are shown in Figure 3-1, Figure 3-2 and Table 3-1 where only a portion of the complete cylinder is shown.

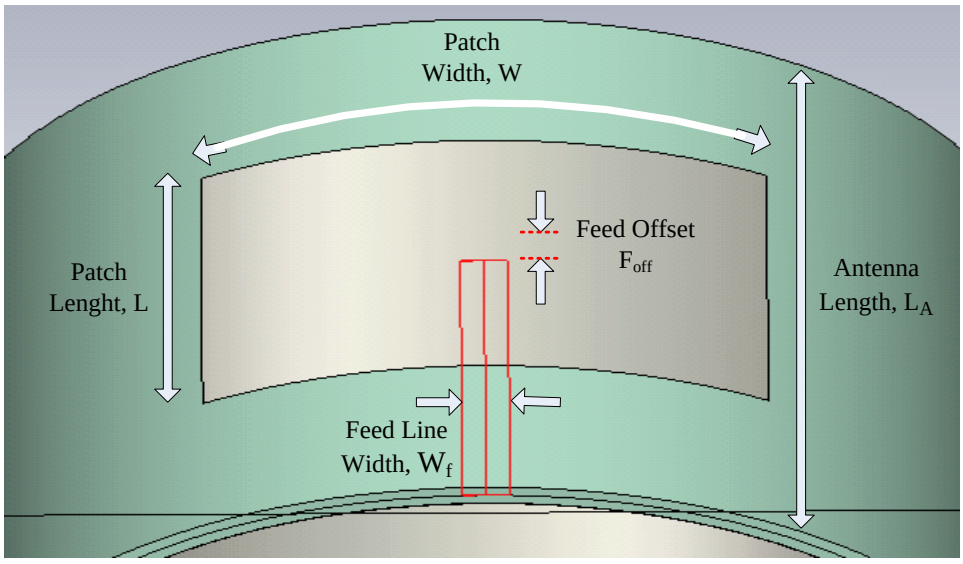

Figure 3-1 Geometry of proximity coupled conformal microstrip antenna - top view

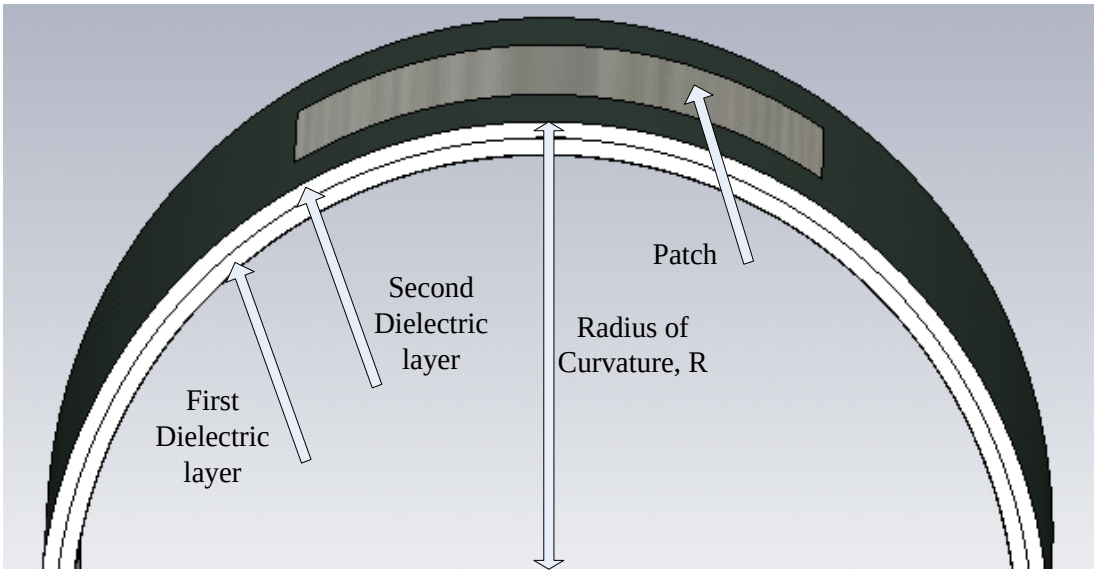

Figure 3-2 Geometry of proximity coupled conformal microstrip antenna - side view

Table 3-1 Design parameters of proximity coupled conformal microstrip antenna

Parameter	Value
Patch Length, L	37,9 mm
Patch Width, W	55 mm
Feed Line Width, W_f	4,2 mm
Feed Offset, F_{off}	0
Dielectric Constant, ε_r	2.33
Radius of Curvature, R	60 mm
Height of the First Dielectric Layer, h_1	1.575 mm
Height of the Second Dielectric Layer , h_2	1.575 mm
Antenna Length, L_A	80 mm

In the following subsections the effect of changing the major design parameters in Table 3-1 is observed.

3.1.1 Effect of Changing the Radius of Curvature

In this subsection the effect of varying the radius of curvature on the resonant frequency and radiated fields is observed. The parameterization is performed according to the values given in Table 3-2. Antenna on a planar substrate is represented as infinite radius of curvature. Simulation results are presented as return loss (S_{11}) and E-, H-Plane far field radiation patterns. After performing the parameterization, return loss for R→∞ is plotted in Figure 3-3 while return loss for the other R values are depicted in Figure 3-4.

Table 3-2 Radius of curvature values used in the parameter sweep

Swept parameter	
Radius of Curvature, R	60 mm
	110 mm
	160 mm
	→∞
Other parameters kept constant	

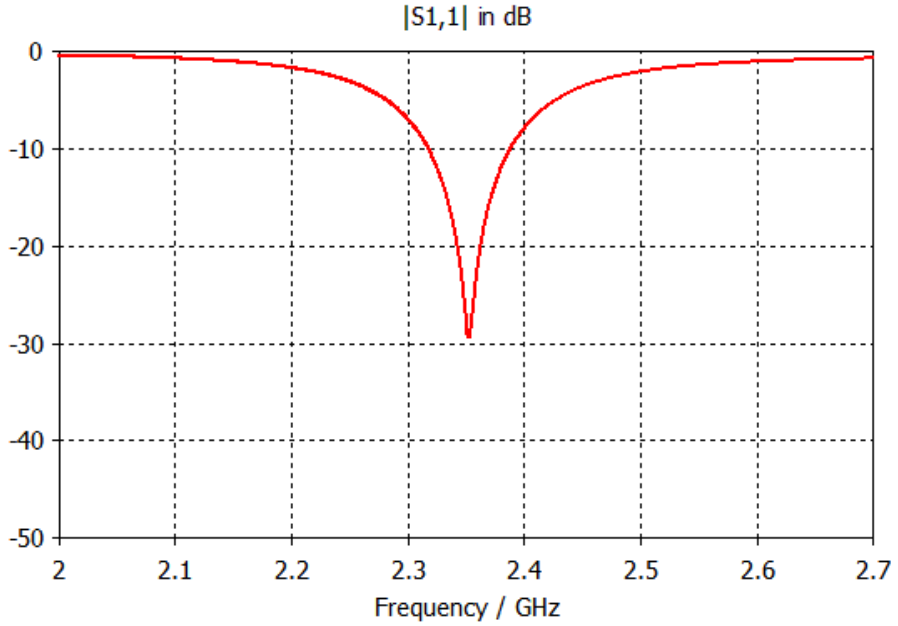

Figure 3-3 Return loss for antenna on a planar substrate (R→∞)

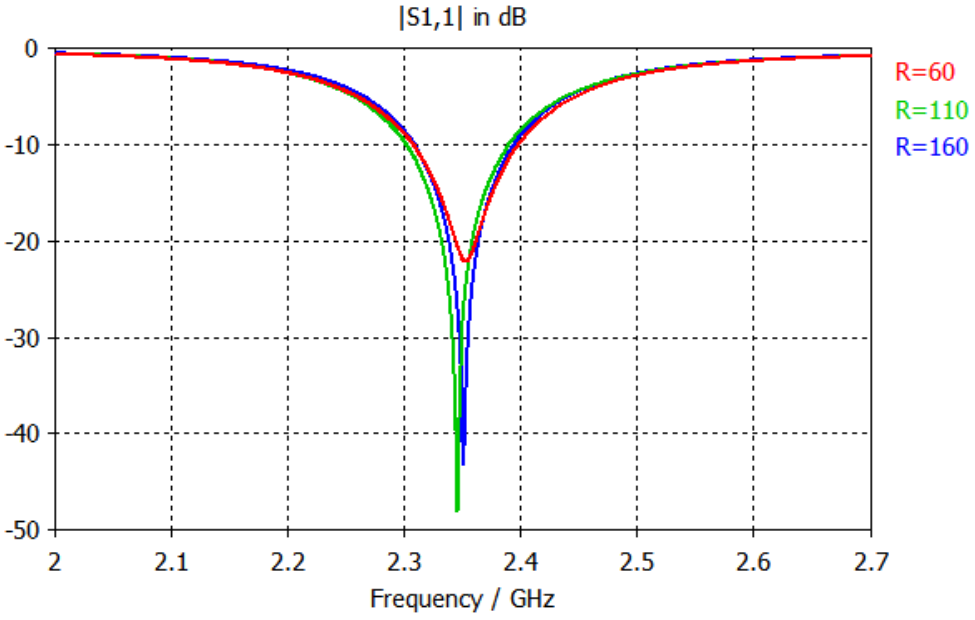

Figure 3-4 Return loss as a function of radius of curvature

It is clear from the figures that resonant frequency changes slightly with the radius of curvature. Also -10 dB bandwidth is increased slightly when the planar antenna is bent or radius of curvature is decreased, which is an expected result [16]. From these observations it can be concluded that, proximity coupled conformal microstrip antenna with a given resonant frequency and bandwidth can be designed in its planar form as an initial design step. After the bending, some very small tunings shall be performed in order to finalize the design.

The effect of changing the radius of curvature on co-polar radiated fields is shown from Figure 3-5 to Figure 3-8. The curved antenna has a higher back radiation than the planar antenna for both E- and H-Planes and back radiation increases as the radius of curvature decreases, as expected. The increase on back radiation is higher for H-Plane because bending is performed on that plane. On the other hand, very small changes are observed on the main lobe radiation when the radius of curvature changes as expected [14]. Antenna gain decreases slightly and coverage on H-plane increases when the curvature radius decreases.

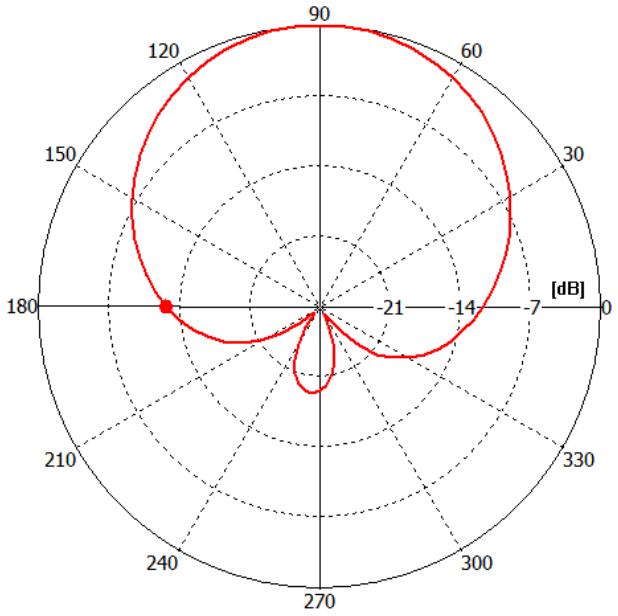

Figure 3-5 E-Plane radiation pattern for antenna on a planar substrate at 2.35 GHz

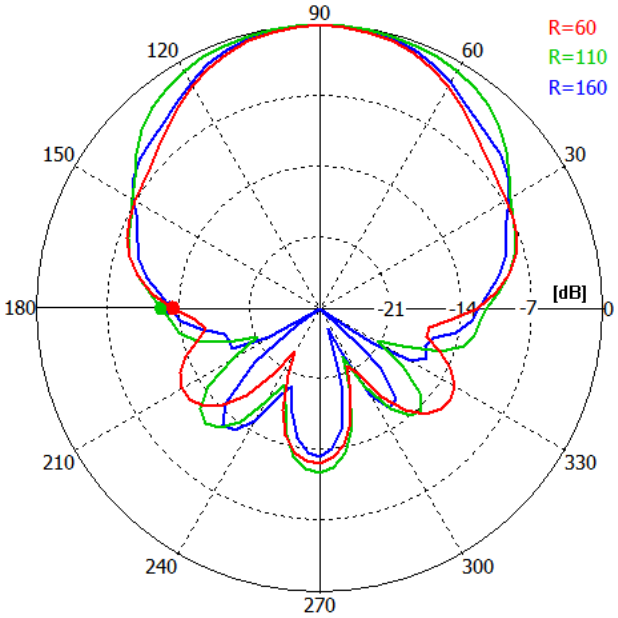

Figure 3-6 E-Plane radiation pattern as a function of curvature radius at 2.35 GHz

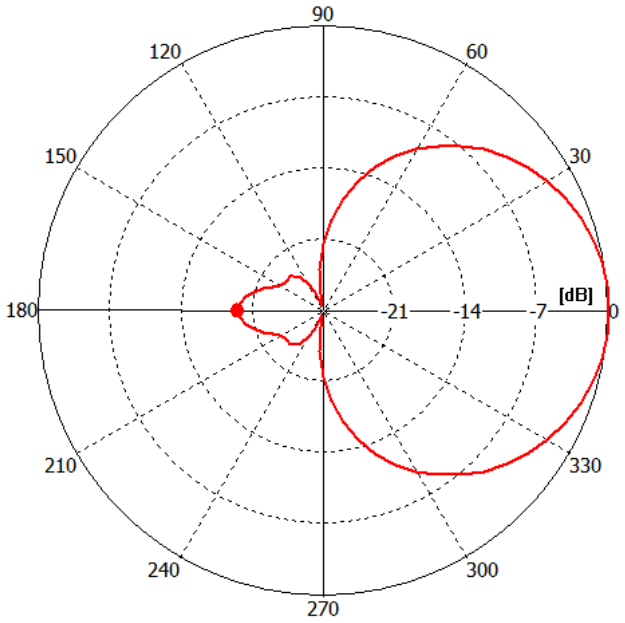

Figure 3-7 H-Plane radiation pattern for antenna on a planar substrate at 2.35 GHz

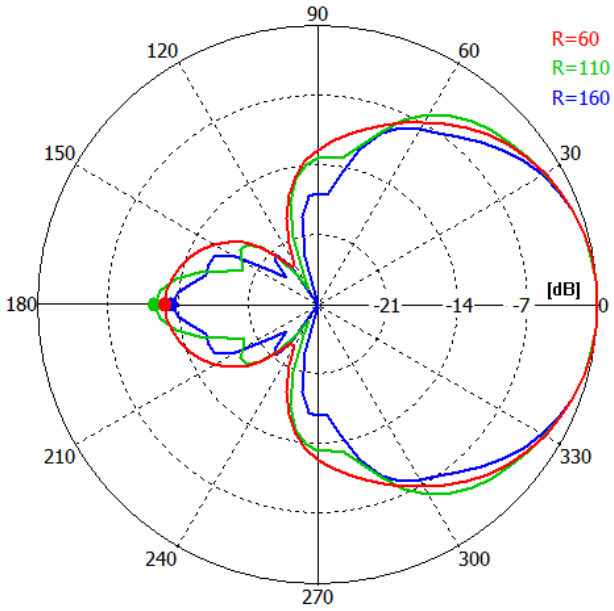

Figure 3-8 H-Plane radiation pattern as a function of curvature radius at 2.35 GHz

3.1.2 Effect of Changing the Feed Offset

In this subsection, input impedance and resonant frequency variations with respect to feed offset changes are investigated. For the feed offset values in Table 3-3, the simulation results are illustrated in Figure 3-9 and Figure 3-10.

Table 3-3 Feed offset values used in the parameter sweep

Swept parameter	
Feed Offset, F_{off}	-4 mm
	-2 mm
	0 mm
	2 mm
	4 mm
Other parameters kept constant	

Increasing the feed offset increases the resonant frequency slightly and rotates the locus of the input impedance in clockwise direction. The same effect is also observed in [5] and [26]. Feed offset value can be used to match the antenna to the feed line easily.

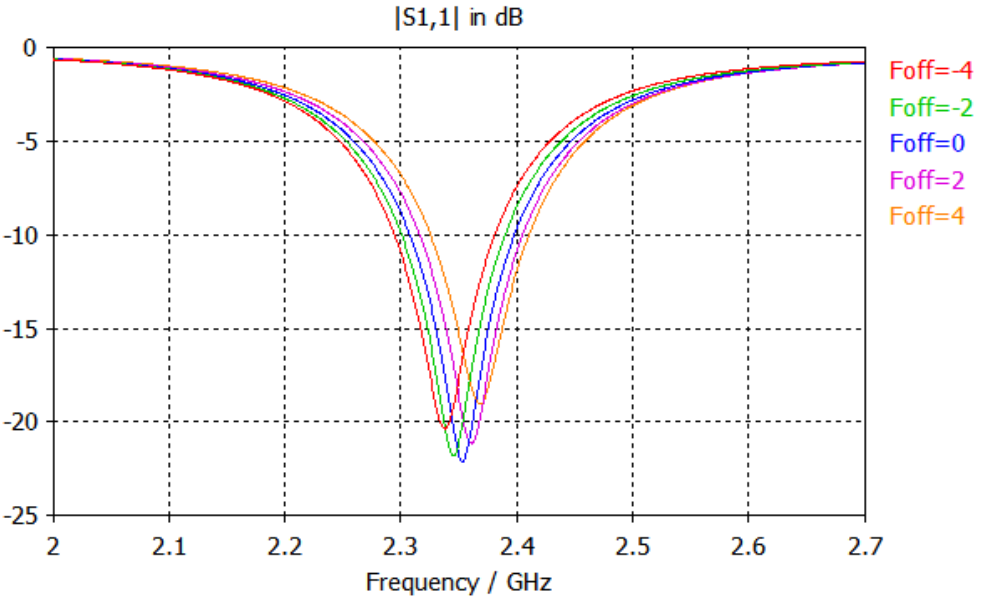

Figure 3-9 Return loss for different values of feed offset

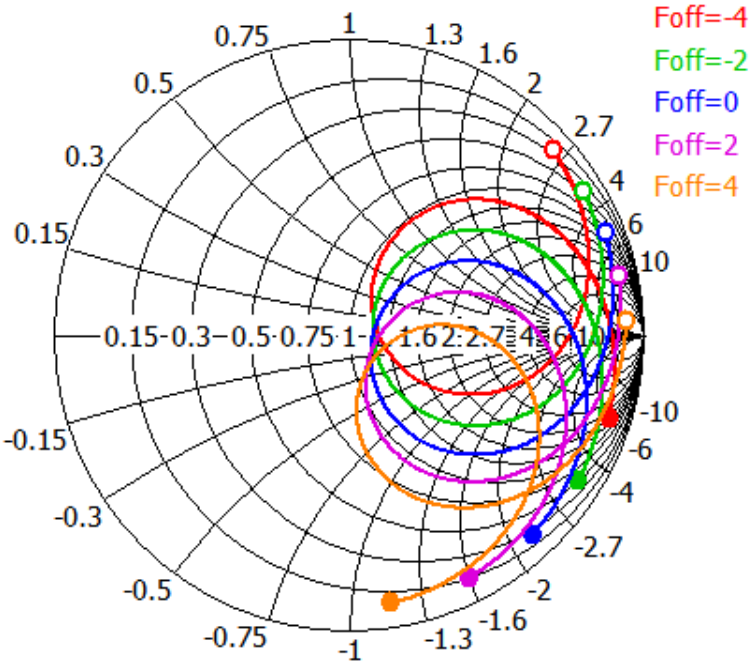

Figure 3-10 Input impedance as a function of feed offset

3.1.3 Effect of Changing the Patch Width

In this subsection, the effect of changing the patch width on the input impedance and resonant frequency is observed. Patch width values used in the parametric sweep are listed in Table 3-4 and the results are presented in Figure 3-11 and Figure 3-12.

Table 3-4 Patch width values used in the parameter sweep

Swept parameter	
Patch Width, W	45 mm
	50 mm
	55 mm
	60 mm
	65 mm
Other parameters kept constant	

As patch width increases, the radius of impedance circle decreases and thus bandwidth increases. This is due to the fact that power radiated increases when patch width increase [4]-[5]. However, there is a practical limit on W, beyond which the cross polarization level is very high. Also, it is observed that increasing the patch width has a decreasing effect on the resonant frequency. This is the result of the increase in the effective length of the patch as the patch width increases. As a result, patch width can be used to adjust the

bandwidth and resonant frequency of the antenna. Such as feed offset, patch width is another means of matching the antenna to the feed line.

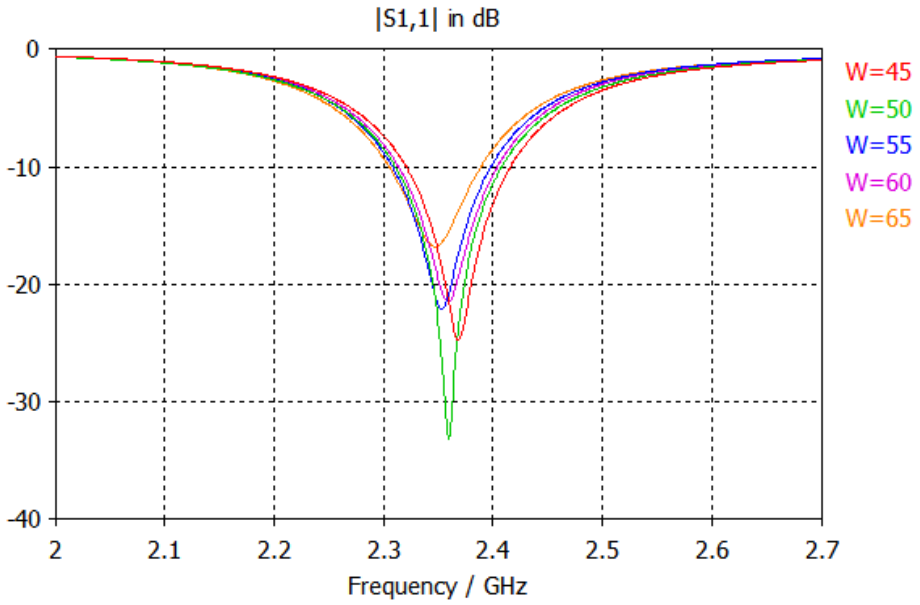

Figure 3-11 Return loss as a function of patch width

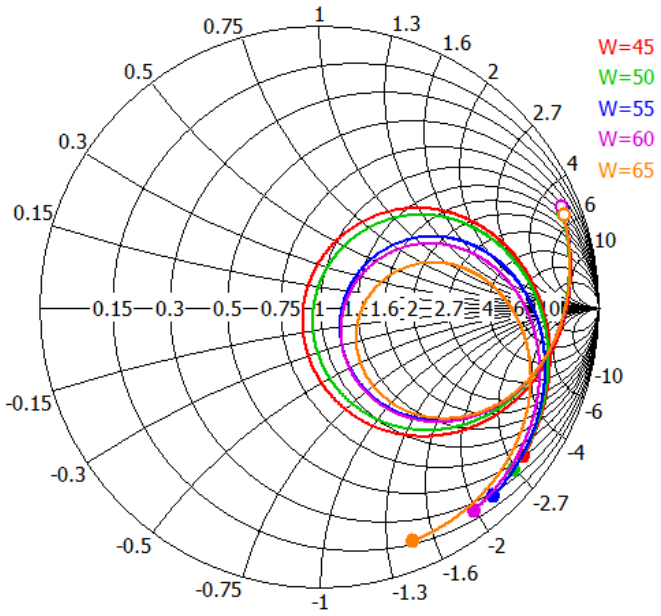

Figure 3-12 Input impedance as a function of patch width

3.2 Design of Proximity Coupled Conformal Microstrip Antenna Arrays

The parametric study in the previous section gave valuable information about the design parameters of the antenna. By using this information and previously designed microstrip antenna element, two different cylindrically conformal array configurations are realized in this section. Radius of curvature values, element spacing and element numbers differ for the two structures. These two arrays operate at a resonance frequency of 2.35 GHz and have omnidirectional radiation pattern in the circumferential plane of the cylinder. Element numbers of the arrays are selected as four and eight respectively to simplify power divider design for these structures. The results of the antennas are given in the following subsections.

3.2.1 Four Element Antenna Array Design

Design parameters of an array element are the same with the parametrically studied antenna and listed in Table 3-1. The geometry of the array is given Figure 3-13. Element spacing, D is 40 mm and the antenna is axially polarized. The same substrate in previous section, Arlon IsoClad 933, is used with a standard thickness of 0.062 inch (1.575mm) and electrodeposited copper of 2 oz (0.07mm). All elements of the array are excited with equal amplitude and phase.

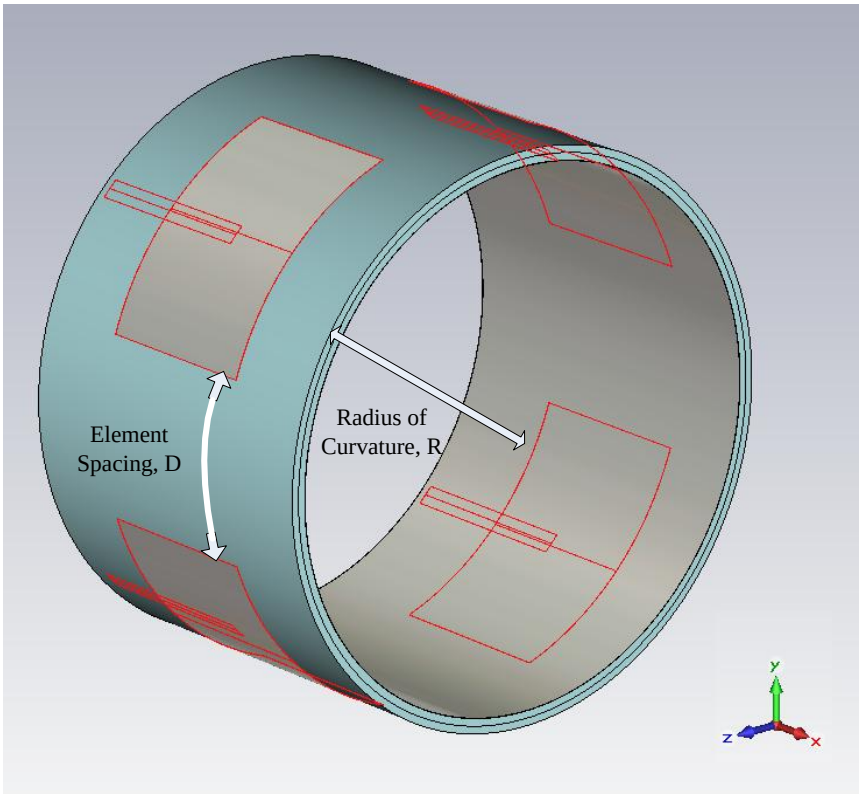

Figure 3-13 Geometry of the four element array

Return loss for one element of the array is provided in Figure 3-14. Since the elements are identical, they all have the same return loss characteristics. The resonant frequency is 2.35 GHz and bandwidth is approximately 110 MHz. The bandwidth is slightly increased as compared to the case when only one element is excited, which is probably due to mutual coupling effects.

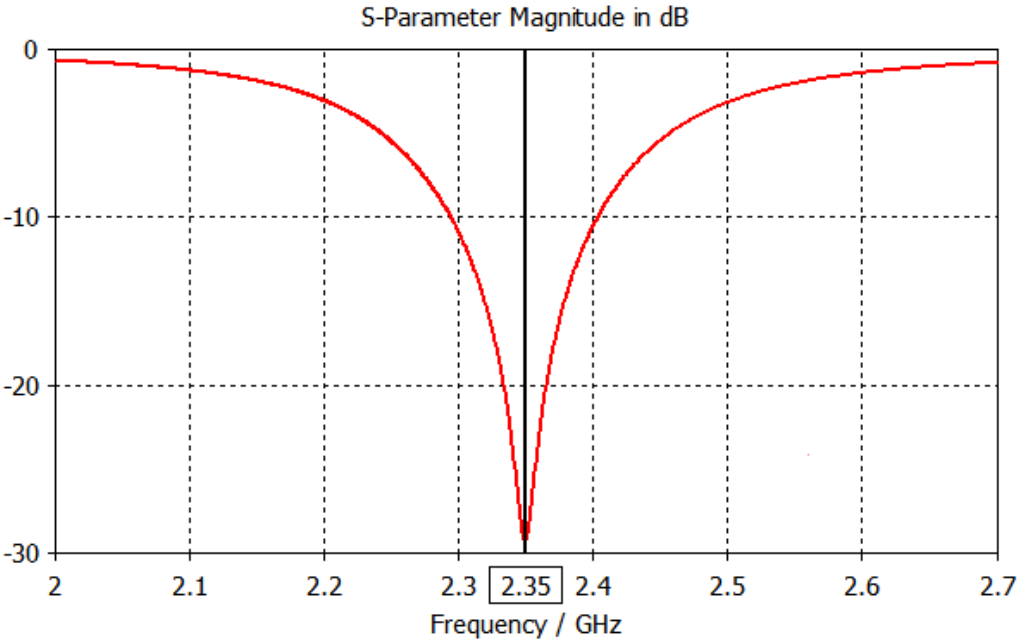

Figure 3-14 Return loss of a single element of the four element array

Far field radiation pattern for axial polarization at 2.35 GHz in the y-z plane is as in Figure 3-15. From the figure it is clear that, in the y-z plane (circumferential plane), the antenna has omnidirectional radiation, which is suitable for rotating vehicles. Peak directivity is 3.65 dB and it occurs just on the mid-point between two patches. The lowest directivity is -1 dB and it happens on the center of each patch. This may be due to the very small radius of curvature. The highest cross-polarization component is less than -30 dB in this plane.

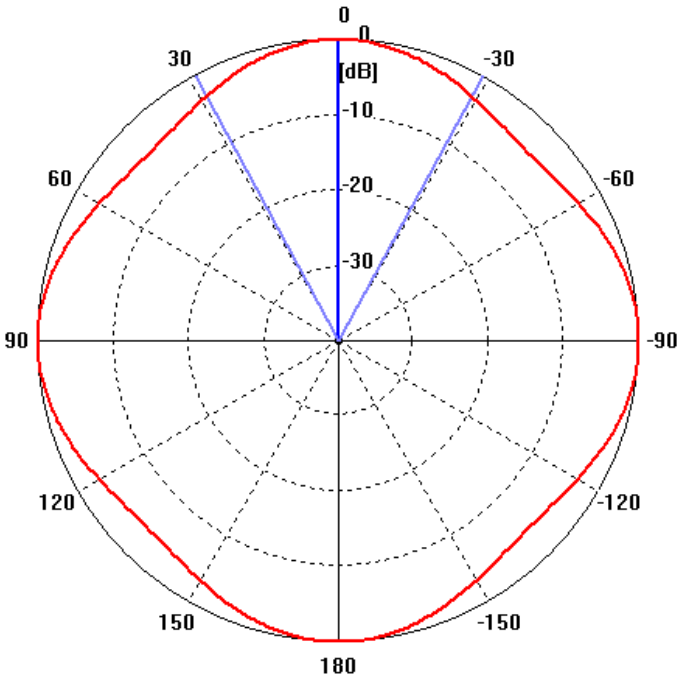

Figure 3-15 Far field radiation pattern in the y-z plane at 2.35 GHz

Far field radiation patterns for axial polarization at 2.35 GHz in the x-z and x-y planes are depicted in Figure 3-16 and Figure 3-17, respectively. For both figures, two zeros occur in x axis and maximum directivity is 3.65 dB. The highest cross-polarization component in both planes is less than -50 dB. The hemispherical coverage is suitable for vehicles that have high maneuver capability. The green lines on the figures indicate the side lobe level.

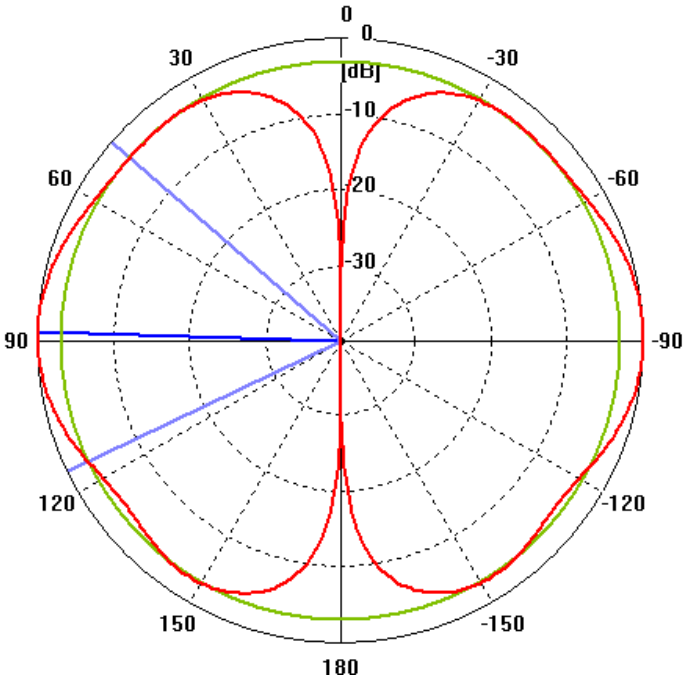

Figure 3-16 Far field radiation pattern in the x-z plane at 2.35 GHz

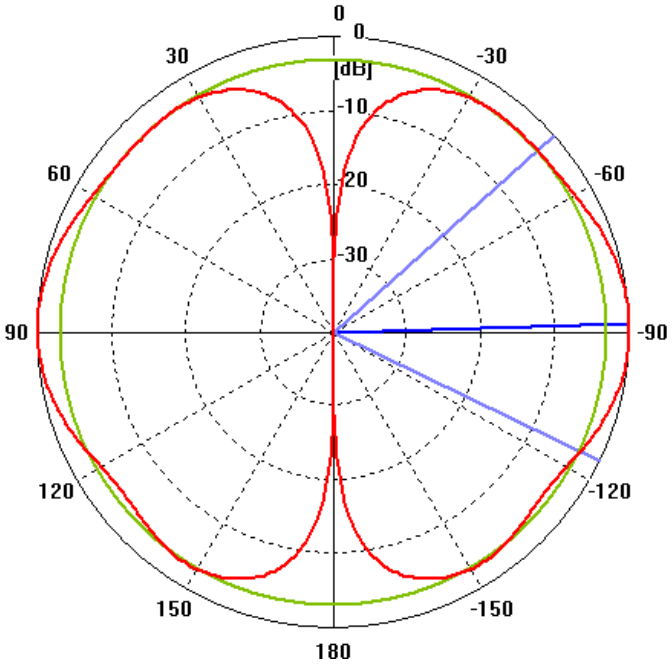

Figure 3-17 Far field radiation pattern in the x-y plane at 2.35 GHz

3.2.2 Eight Element Antenna Array Design

The design parameters are same with the previous four element array except R=135 mm and D=51 mm in this case. Each element is excited with the same amplitude and phase. Geometry of the antenna is given in Figure 3-18.

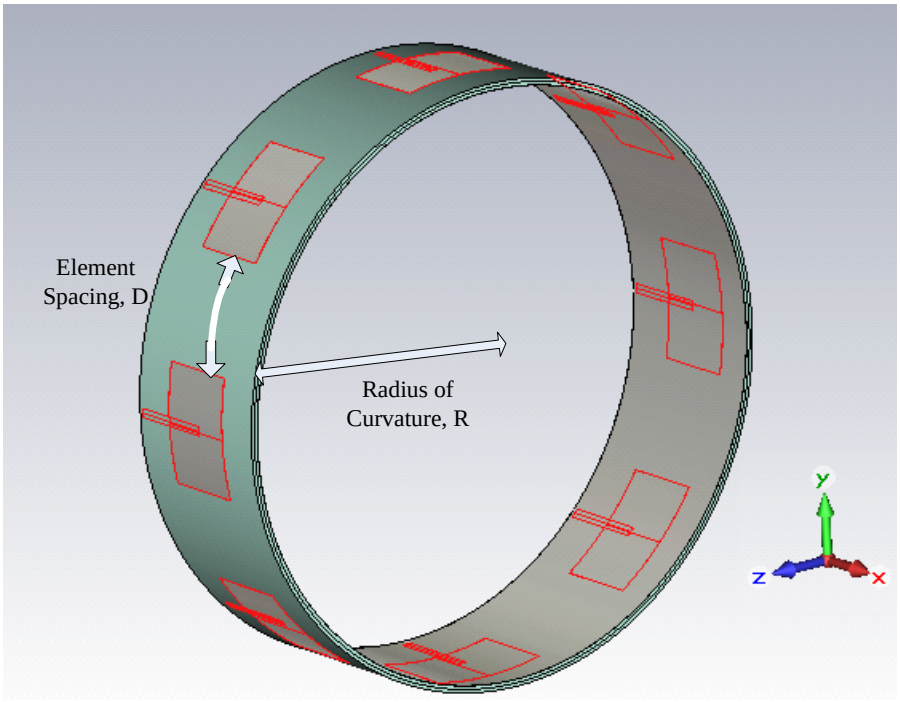

Figure 3-18 Geometry of the eight element array

Return loss for one element of the array is shown in Figure 3-19. There is no doubt that all elements have the same return loss characteristics. Resonant frequency is 2.35 GHz and bandwidth is 90 MHz. As in the case of four element array, bandwidth is slightly increased when compared to only one element excited case. Mutual coupling effect is probably the underlying reason of this behavior.

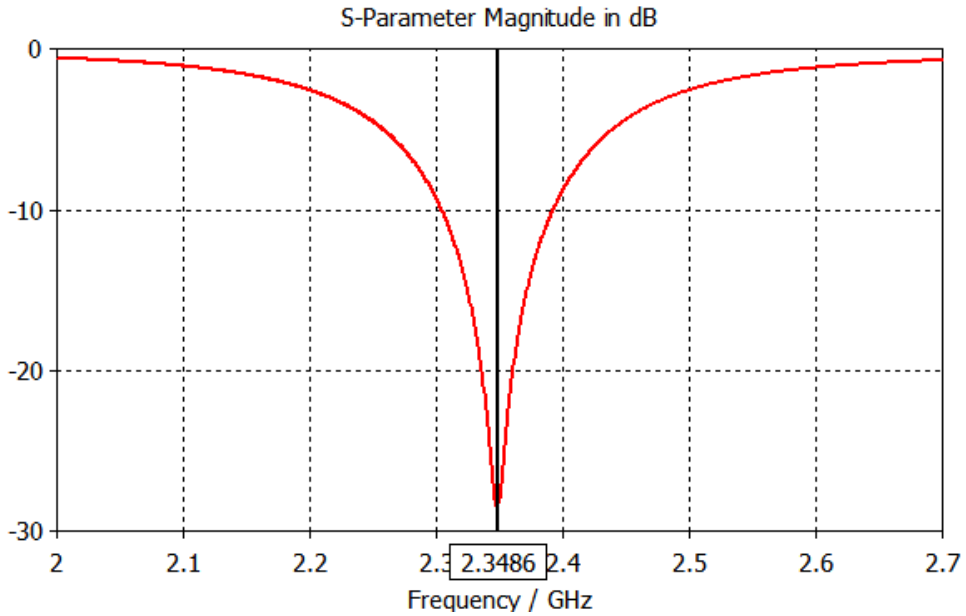

Figure 3-19 Return loss of a single element of the eight element array

Figure 3-20 is the result of far field radiation pattern in the y-z plane for axial polarization. The radiated field in this plane is omnidirectional with a minimum directivity of 0.6 dB and maximum directivity of 3.8 dB. Maxima occur on the center of each patch while minima are on the mid-point between two patches. The highest cross-polarization component is -28 dB in this plane.

Far field radiation patterns for axial polarization in the x-z and x-y planes are plotted in Figure 3-21 and Figure 3-22, respectively. For both figures, two zeros occur in x axis and maximum directivity is 3.8 dB. The highest cross-polarization component in both planes is less than -60 dB. Again the hemispherical coverage is very useful for vehicles that have high maneuverability. The green lines on the figures indicate the side lobe level.

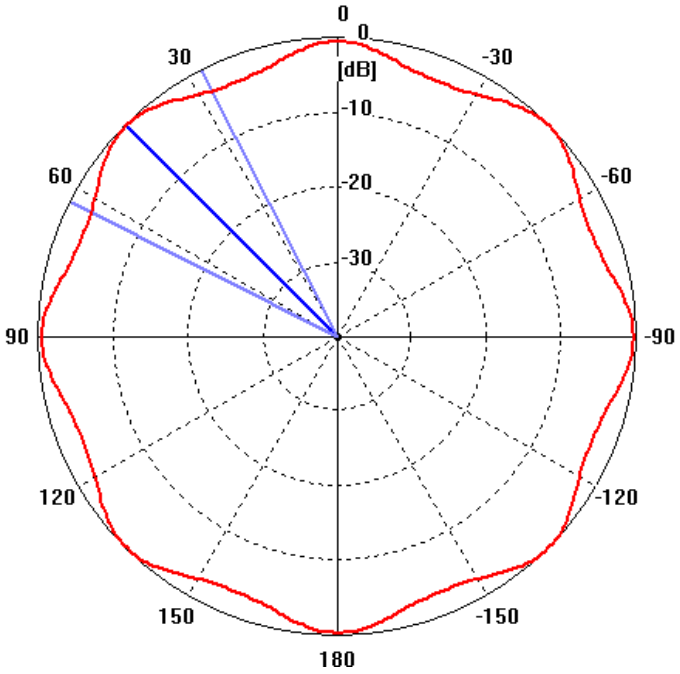

Figure 3-20 Far field radiation pattern in the y-z plane at 2.35 GHz

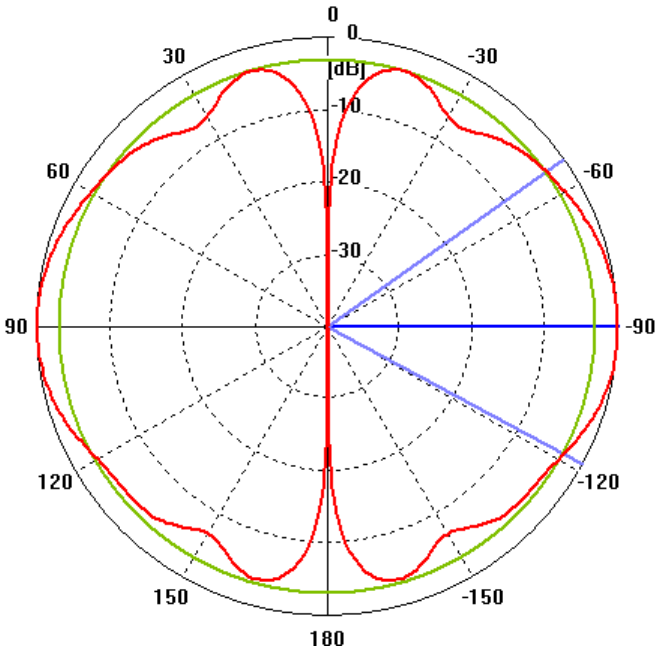

Figure 3-21 Far field radiation pattern in the x-z plane at 2.35 GHz

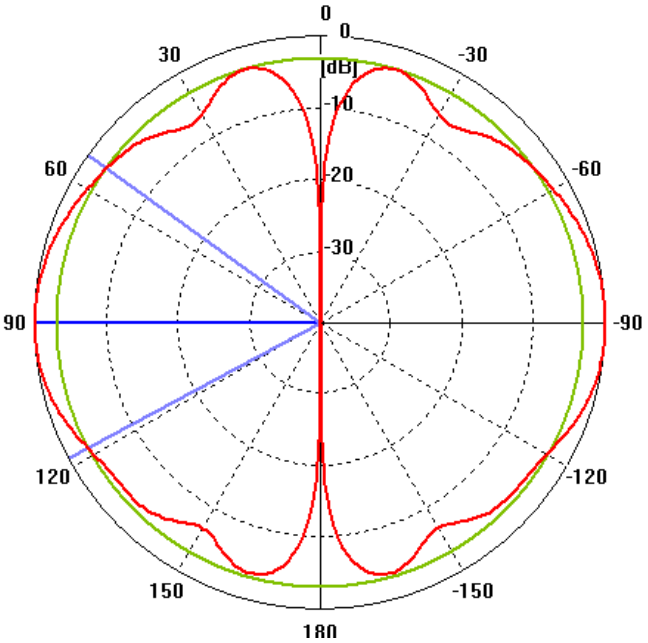

Figure 3-22 Far field radiation pattern in the x-y plane at 2.35 GHz

3.3 Conclusions

In this chapter parametric analysis of a proximity coupled cylindrically conformal antenna is carried out. The effect of important design parameters is analyzed and with the help of this analysis two different conformal arrays are realized. Both arrays have omnidirectional radiation in the circumferential plane and hemispherical coverage in the other two planes. These two arrays have very compact structure and are suitable for airborne applications. Bandwidth of the antennas is around %4, which is sufficient for telemetry and some data-link applications. However, for communication systems having electronic counter-counter measure this bandwidth may be low and it should be enhanced in order to increase the resistance to electronic warfare.

CHAPTER 4

ANALYSIS AND DESIGN OF E-SHAPED CYLINDRICALLY CONFORMAL MICROSTRIP ANTENNA ARRAYS

In this chapter, parametric analysis of E-shaped cylindrically conformal microstrip antenna element operating in the 1.9-2.55 GHz band is performed initially. This frequency range is useful in modern wireless communications. After that, two different E-Shaped conformal microstrip antenna arrays are designed and analyzed in the aforementioned band. Simulation method is verified at the end of this chapter. As in the previous chapter, simulations are performed in CST MICROWAVE STUDIO®.

4.1 Parametric Analysis of E-Shaped Conformal Microstrip Antenna Element

In this part, a parametric study is performed with an E-shaped cylindrically conformal microstrip antenna to gain information about the design parameters. Flexible Arlon IsoClad 933 substrate is used as in the previous chapter. In order to achieve the required bandwidth, six layers of the material are used with each layer having a standard thickness of 0.062 inch (1.575mm). Between any two layers Arlon CuClad 6700 bonding film is used with a thickness of 0.006 inch (0.1524mm), which has the same dielectric constant with the substrate. After the process, the substrate has overall thickness of

10.212 mm and electrodeposited copper of 2 oz (0.07mm). The inner radius of the 50 Ω SMA coaxial probe is 0.635 mm while the outer radius is 2.05mm. Feed line is located below the W/2 line to make the antenna axially polarized. Antenna design parameters are given in Figure 4-1, Figure 4-2 and Table 4-1 where only a portion of the complete cylinder is shown.

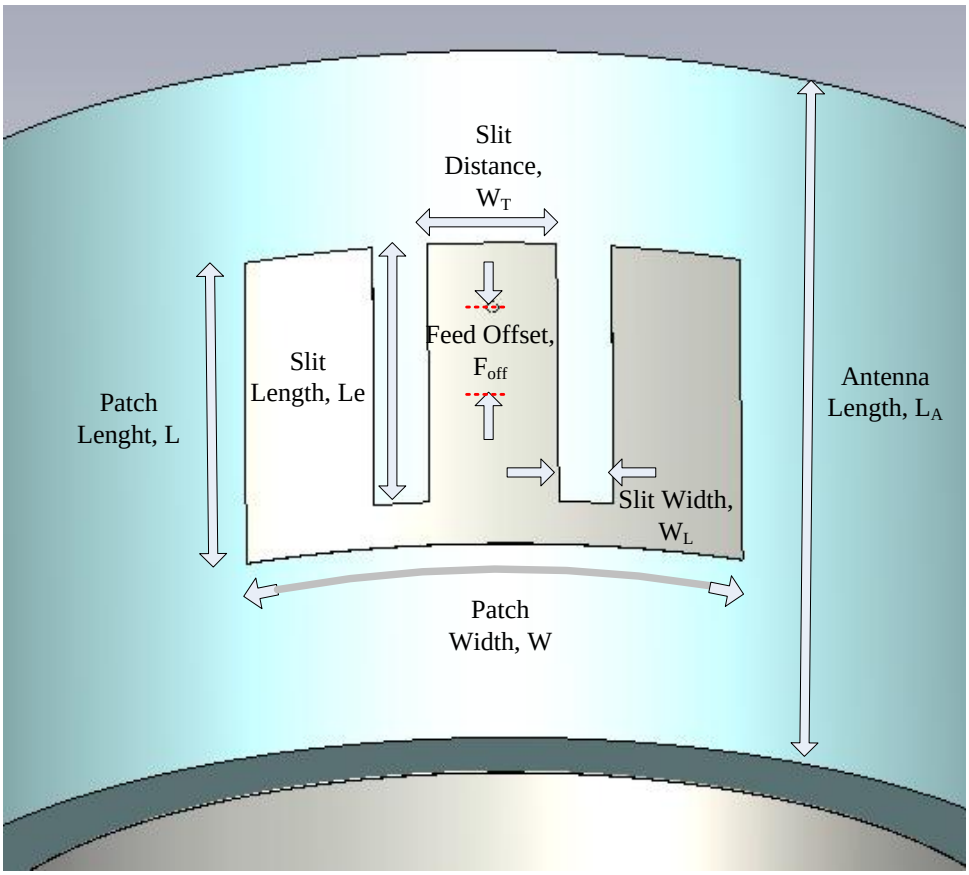

Figure 4-1 Geometry of E-shaped conformal microstrip antenna - top view

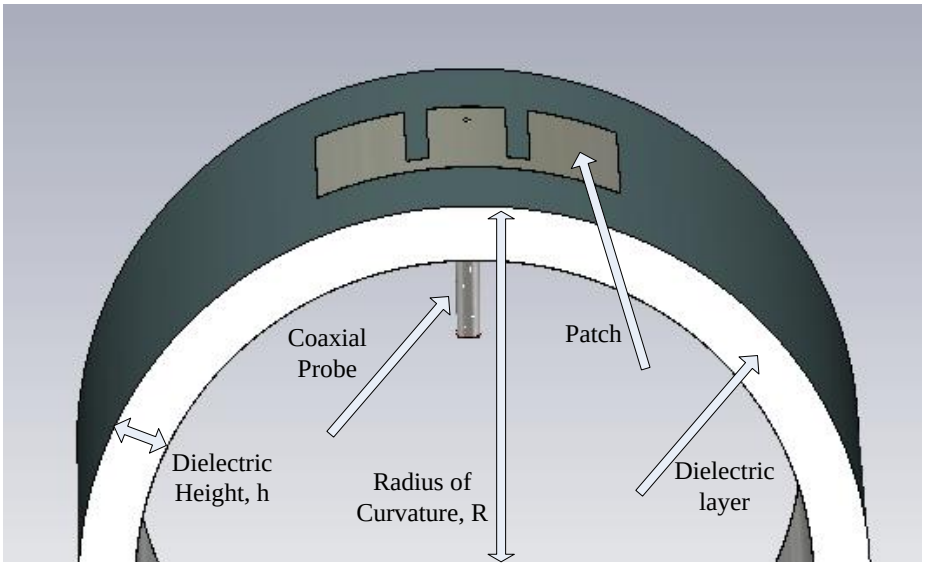

Figure 4-2 Geometry of E-shaped conformal microstrip antenna - side view

Table 4-1 Design parameters of the E-shaped conformal microstrip antenna

Parameter	Value
Patch Length, L	35 mm
Patch Width, W	55 mm
Slit Length , L_e	30 mm
Slit Width, W_L	9 mm
Slit Distance, W_T	14 mm
Feed Offset, F_{off}	10 mm
Dielectric Constant, ε_r	2.33
Radius of Curvature, R	70 mm
Height of the Dielectric Layer, h	10.212 mm
Inner Radius of the Coaxial Probe, F_{in}	0.635 mm
Inner Radius of the Coaxial Probe, F_{out}	2.05 mm
Antenna Length, L_A	80 mm

In the following subsections, the effect of changing the major design parameters in Table 4-1 is observed. In each parametric study, one variable is changed while keeping the others constant.

4.1.1 Effect of Changing the Radius of Curvature

The effect of varying the radius of curvature on the resonant frequency and radiated fields is investigated in this section. Antenna on a planar substrate is represented as infinite radius of curvature. Simulation results are presented as return loss (S_{11}) and E-, H-Plane far field radiation patterns. The parameterization is performed according to the values given in Table 4-2 and corresponding return loss values are depicted in Figure 4-3 and Figure 4-4.

Table 4-2 Radius of curvature values used in the parameter sweep

Swept parameter	
Radius of Curvature, R	70 mm
	120 mm
	170 mm
	$\rightarrow \infty$
Other parameters kept constant	

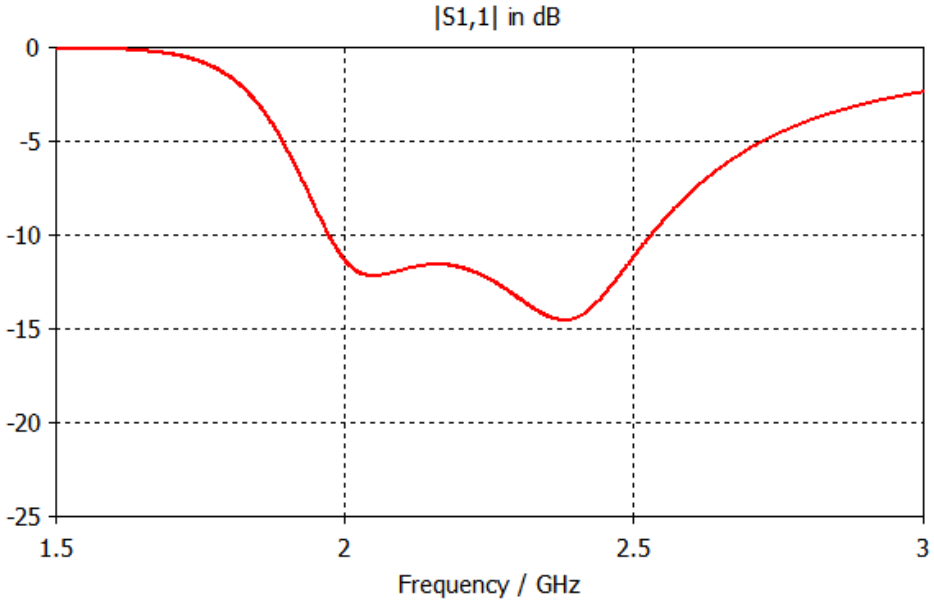

Figure 4-3 Return loss for antenna on a planar substrate (R→∞)

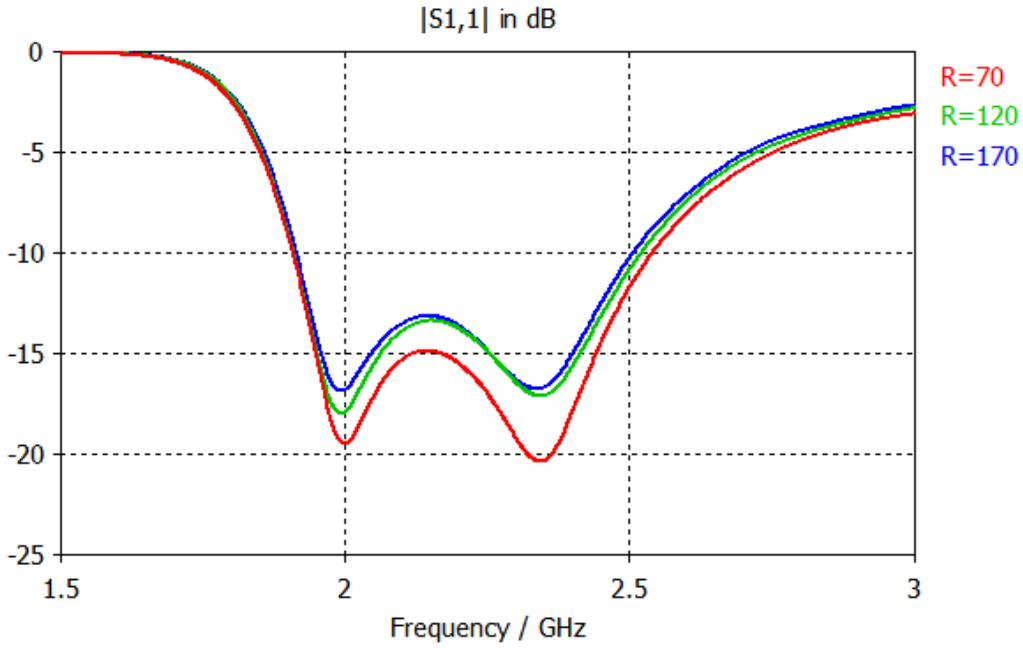

Figure 4-4 Return loss for different values of radius of curvature

It is clear from the figures that radius of curvature has a slight effect on return loss of the antenna. The slight effect is an increase in the -10 dB bandwidth when the radius of curvature is decreased. The same effect is also observed for another type of compact broadband structure in [15].

The effect of changing the radius of curvature on co-polar radiated fields is shown from Figure 4-5 to Figure 4-8. For both planes, main lobe does not change significantly with the radius of curvature. The minor effect in main lobe is a slight decrease in directivity. On the other hand, back radiation is higher for E- and H-plane for curved antenna when compared with the planar one. Back radiation increases as radius of curvature decreases for E- plane; however for H-plane it remains nearly the same as curvature changes. The back radiation due to slits create asymmetry on the back radiated field for E-Plane and back radiation is higher just below the slits for that reason. In addition, maximum of the main lobe on E-Plane shifts slightly for E-shaped antenna when compared to regularly shaped microstrip antennas, which is again because of the effect of slits on the surface currents of the antenna.

From the above observations it is clear that, E-shaped cylindrically conformal microstrip antenna can be designed in its planar form to simplify the analysis and design process. After that, the antenna can be tuned for the cylindrical operation.

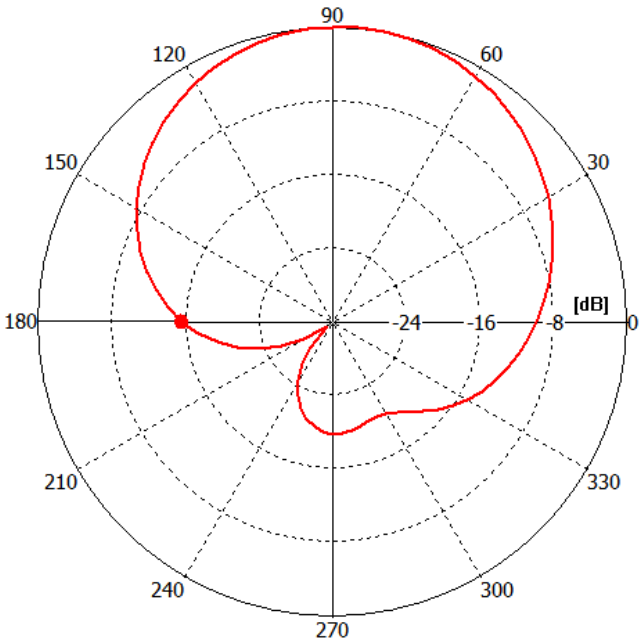

Figure 4-5 E-Plane radiation pattern for antenna on a planar substrate at 2.25 GHz

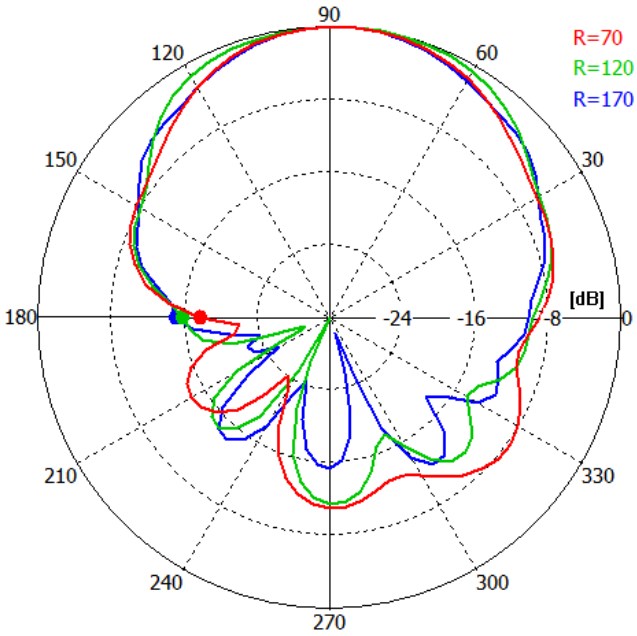

Figure 4-6 E-Plane radiation pattern as a function of curvature radius at 2.25 GHz

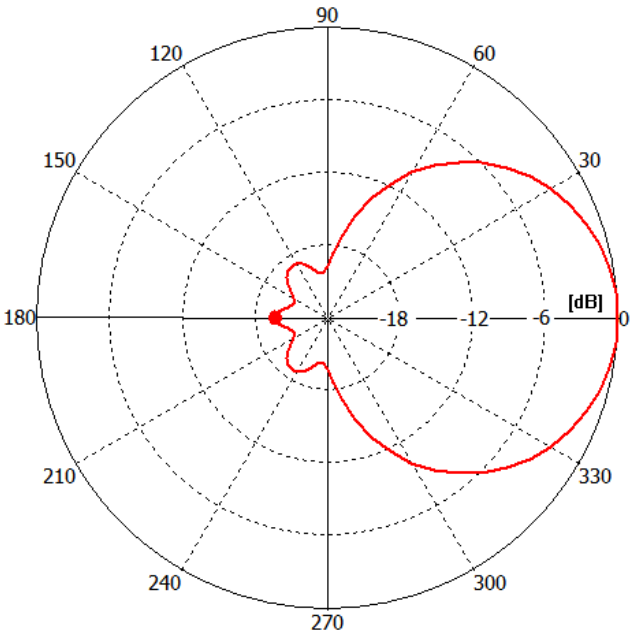

Figure 4-7 H-Plane radiation pattern for antenna on a planar substrate at 2.25 GHz

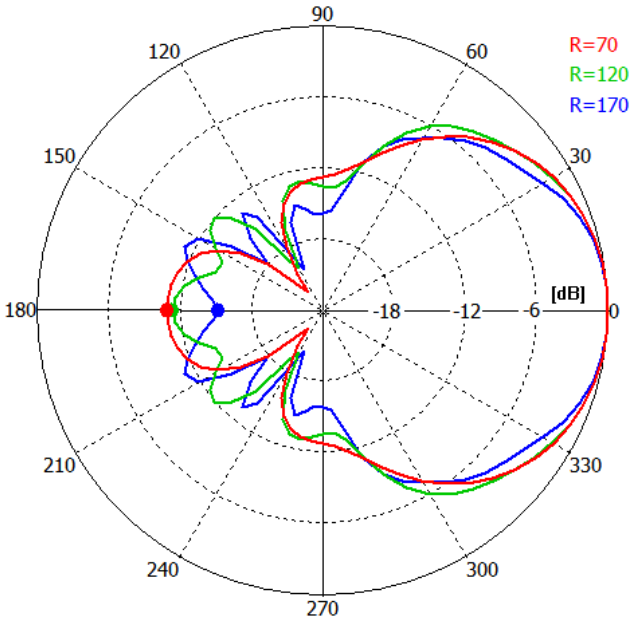

Figure 4-8 H-Plane radiation pattern as a function of curvature radius at 2.25 GHz

For R=70 mm, current distributions on the patch at 1.9 GHz and 2.55 GHz are plotted in Figure 4-9 and Figure 4-10. At 1.9 GHz, currents are mainly concentrated around the slits. The opposite current directions around the outer and inner edge of each slits indicate that this resonance is dominated by the slits. However, at 2.55 GHz the currents are directed along the length of the patch, which shows that this resonance is dominated by the patch [34].

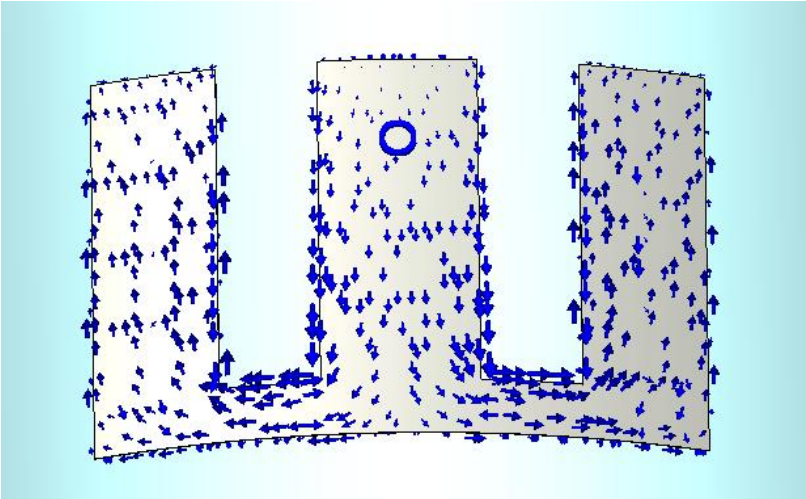

Figure 4-9 The current distribution on the patch at 1.9 GHz

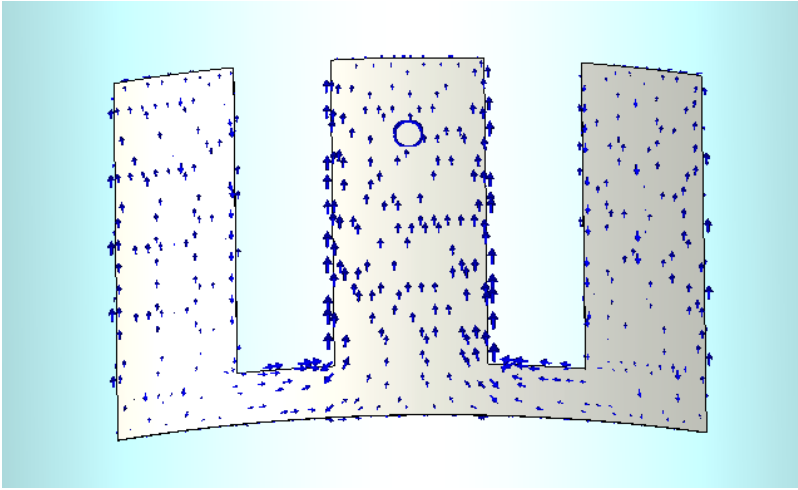

Figure 4-10 The current distribution on the patch at 2.55 GHz

4.1.2 Effect of Changing the Slit Length

In this subsection, the effect of changing the slit length on the input impedance and resonant frequency is investigated. For the feed offset values in Table 4-3, the simulation results are illustrated in Figure 4-11 and Figure 4-12.

Table 4-3 Slit length values used in the parameter sweep

Swept parameter	
Slit Length, L_e	18 mm
	22 mm
	26 mm
	30 mm
	34 mm
Other parameters kept constant	

For small values of slit length, the antenna has only one resonant frequency, the resonant frequency of the patch. When slit length increases, another lower resonant frequency appears and wideband behavior is accomplished. Further increase changes the input impedance and wideband behavior is no longer observed. Slit length is a significant parameter in determining the resonant frequencies of the E-shaped antenna [41].

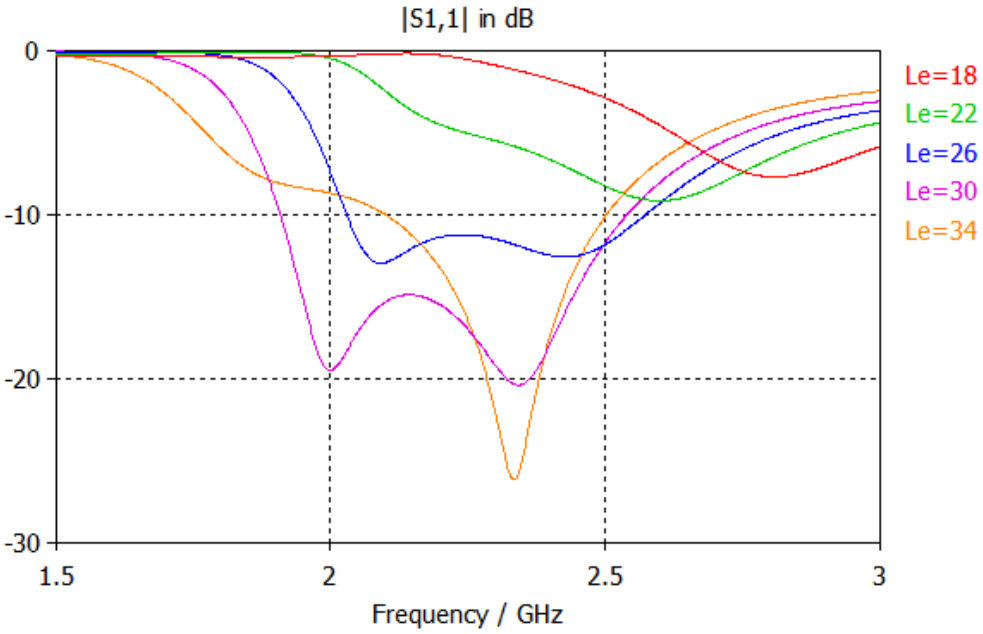

Figure 4-11 Return loss for different values of slit length

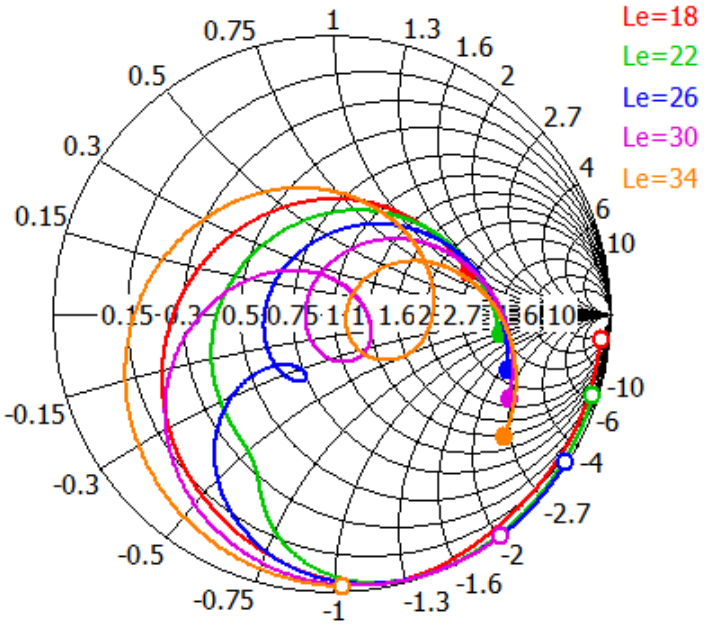

Figure 4-12 Input impedance for different values of slit length

4.1.3 Effect of Changing the Slit Width

The effect of changing the slit width on the input impedance and resonant frequency is analyzed in this section. For the varying parameter values in Table 4-4, results are provided in Figure 4-13 and Figure 4-14.

Table 4-4 Slit width values used in the parameter sweep

Swept parameter	
Slit Width, W_L	3 mm
	6 mm
	9 mm
	12 mm
	15 mm
Other parameters kept constant	

It can be understood from Figure 4-13 that, the two resonant frequencies exist in all five cases, but best matching is for W_L=9 mm. This is due to the fact that slit width changes the radius of the impedance circle on Smith Chart. Therefore, slit width is a useful parameter in adjusting the coupling between the two resonant frequencies and can be used to obtain better matching [41].

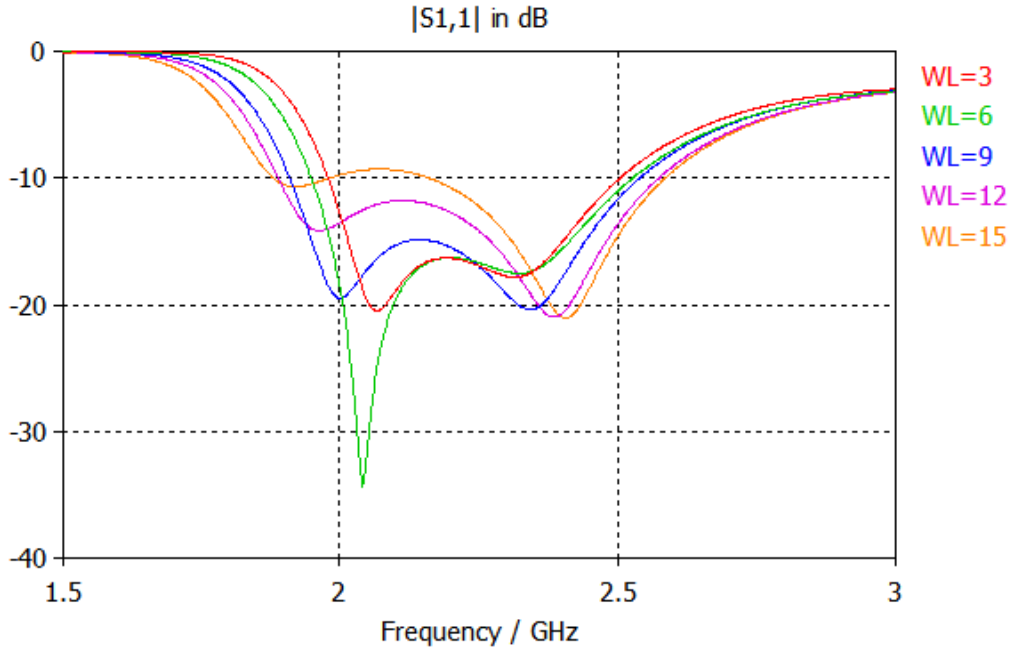

Figure 4-13 Return loss as a function of slit width

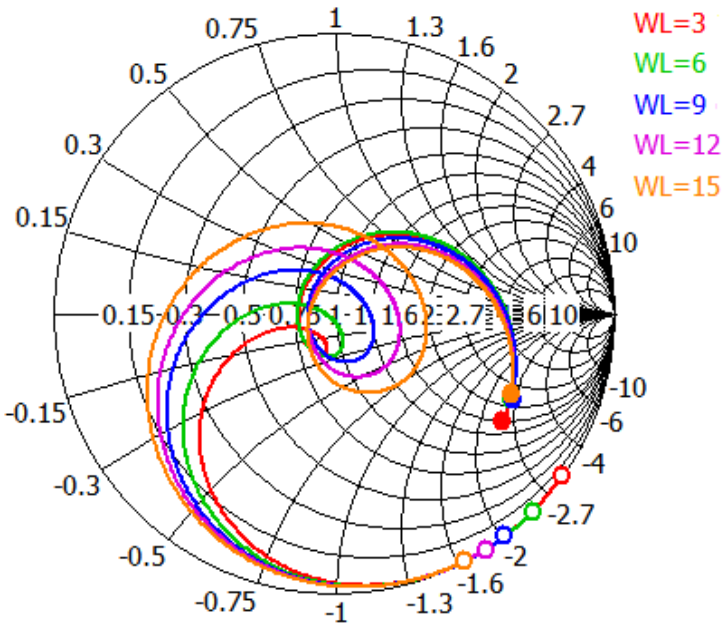

Figure 4-14 Input impedance as a function of slit width

4.1.4 Effect of Changing the Slit Distance

In this subsection, the variations of antenna input impedance and resonant frequency with respect to the slit distance changes are investigated. In Table 4-5, the slit distance values used is listed and the plots in Figure 4-15 and Figure 4-16 show the results.

Table 4-5 Slit distance values used in the parameter sweep

Swept parameter	
Slit Distance, W_T	6 mm
	10 mm
	14 mm
	18 mm
	22 mm
Other parameters kept constant	

For small values of slit distance, the antenna does not show wideband characteristics. However, when slit distance is too large, a wideband characteristic is observed but the antenna does not match to 50 Ω. Therefore it can be concluded that slit distance is a useful parameter to adjust the matching and the bandwidth of the antenna [41].

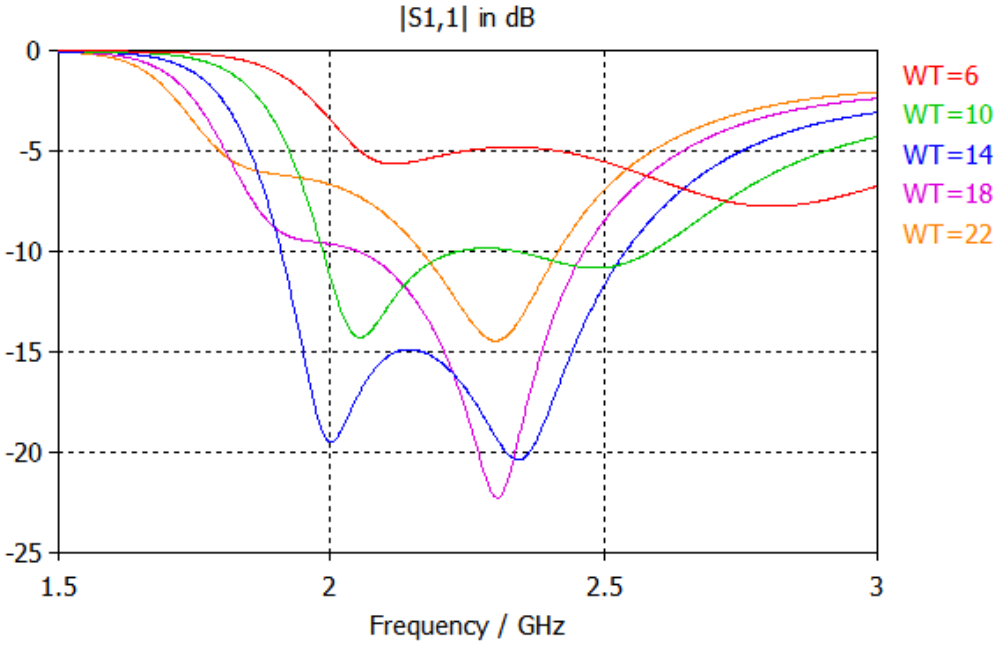

Figure 4-15 Return loss as a function of slit distance

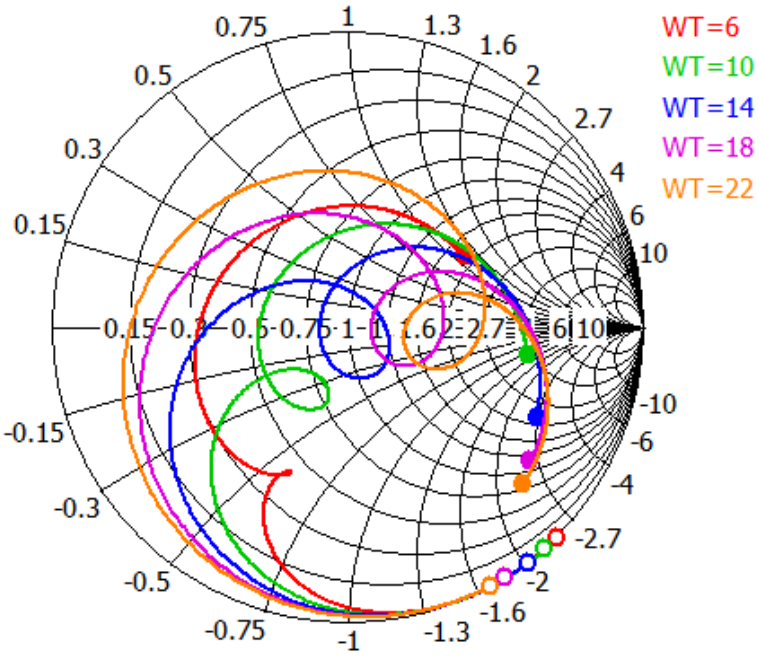

Figure 4-16 Input impedance as a function of slit distance

4.1.5 Effect of Changing the Feed Offset

The effect of feed offset on input impedance and resonant frequency is observed in this section. Table 4-6 shows the feed offset values for which the simulations have been performed and corresponding results are presented in Figure 4-17 and Figure 4-18.

Table 4-6 Feed offset values used in the parameter sweep

Swept parameter	
Feed Offset, F_{off}	6 mm
	8 mm
	10 mm
	12 mm
	14 mm
Other parameters kept constant	

For smaller values of feed offset, the antenna does not have wideband operation. When this value is increased, the two resonant frequencies of the antenna become distinct and wide bandwidth is observed. Further increase in the feed offset causes a dual-band operation, which may be useful for some other applications. Feed offset is another useful variable to control the bandwidth of the antenna.

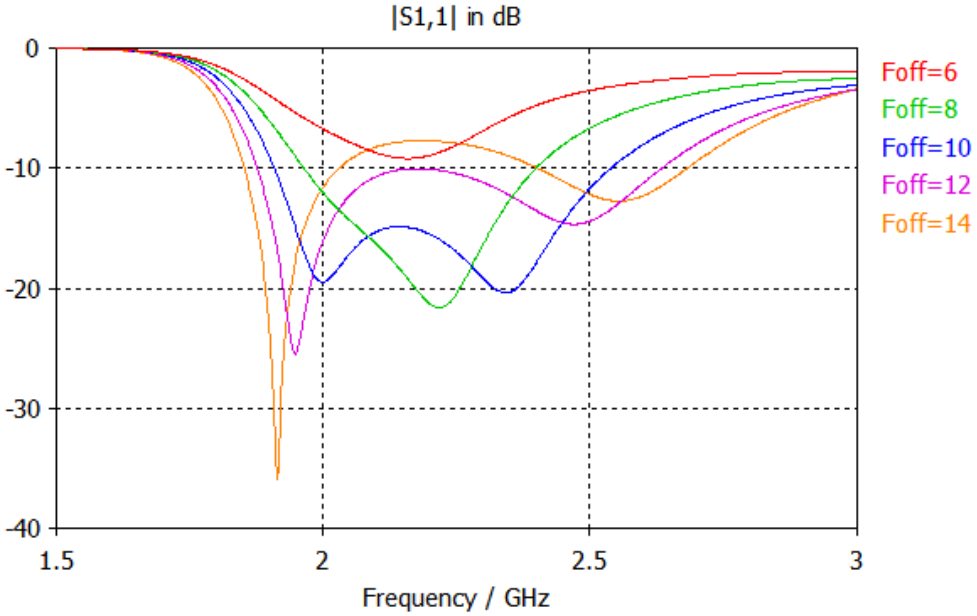

Figure 4-17 Return loss as a function of feed offset

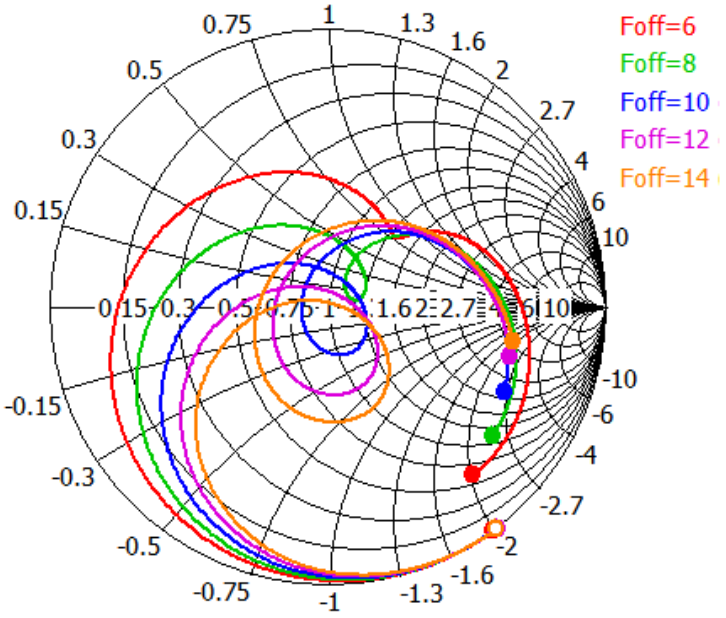

Figure 4-18 Input impedance as a function of feed offset

4.2 Design of E-Shaped Conformal Microstrip Antenna Arrays

With the help of the parametric study in the previous part, two different cylindrically conformal array configurations are designed in this section. Element numbers, element spacing and radius of curvature values are different for the two structures. These two antennas have omnidirectional radiation pattern in the circumferential plane of the cylinder and include the commercial telemetry band. Element numbers of the arrays are selected as four and eight respectively since these numbers are suitable to simplify the power divider design for these structures. Results for the two arrays are presented in the following subsections.

4.2.1 Four Element Antenna Array Design

The same design parameters with the parametrically studied antenna are used for each array element and these parameters are listed in Table 4-1. Array configuration is shown in Figure 4-19. Arlon IsoClad 933 substrate is used with overall thickness of 10.212 mm and electrodeposited copper of 2 oz (0.07mm). Element spacing, D is 55 mm and antenna is axially polarized. Excitation of all elements is with equal amplitude and phase.

Return loss for an array element is plotted in Figure 4-20, which is identical for all elements. The bandwidth, of the antenna is 700 MHz or about 31% with respect to the center frequency at 2.25 GHz. Center frequency is the average of the lower and higher resonant frequencies with -10 dB return loss. Just as in the previous chapter, bandwidth increases when compared to only one element excited case, which is probably a result of mutual coupling.

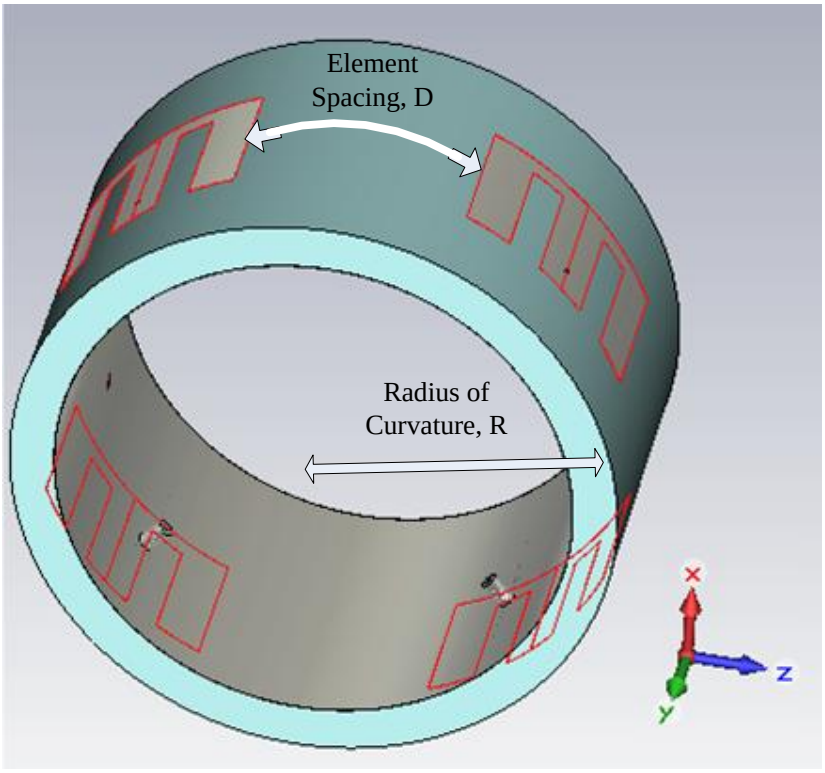

Figure 4-19 Geometry of the four element array

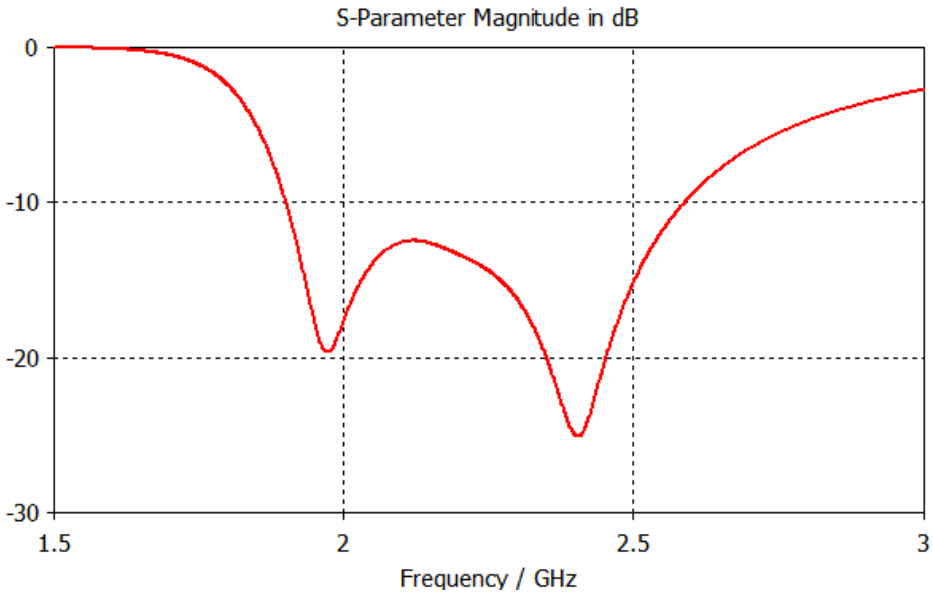

Figure 4-20 Return loss of a single element of the four element array

Far field radiation pattern for axial polarization at 1.9 GHz in the x-z plane is depicted in Figure 4-21. The antenna has an omnidirectional radiation pattern in this plane with -0.5 dB maximum and -3 dB minimum directivities. Maximum cross polarization component in that plane is -10 dB.

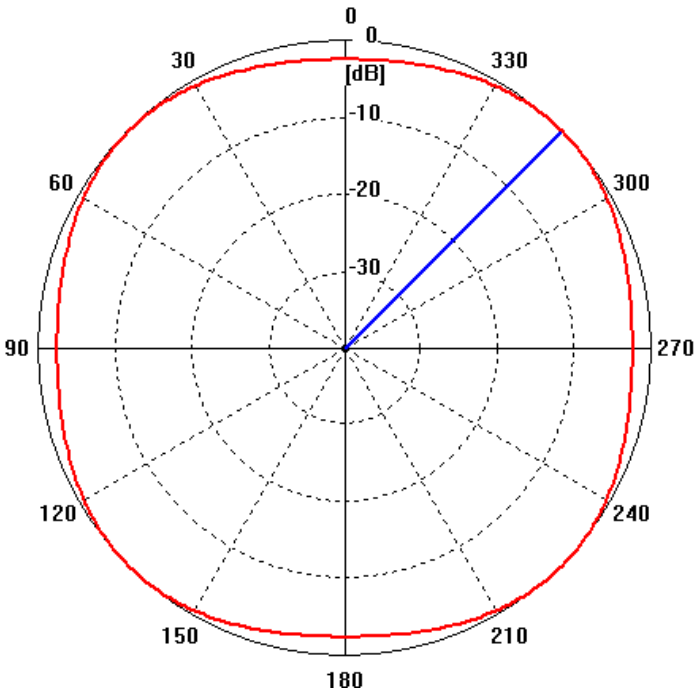

Figure 4-21 Far field radiation pattern in the x-z plane at 1.9 GHz

Figure 4-22 and Figure 4-23 are the results of far field radiation pattern for axial polarization at 1.9 GHz in y-z and x-y planes respectively. For both planes, maximum directivity is 3.8 dB and two nulls occur in y axis. Asymmetry on the hemispheres is due to the disturbance of the slits and maximum directivity is shifted towards the radiating edge of the patch where slits are cut. This is the main reason of the lower gain in x-z plane. Both planes have highest cross polarization components around -60 dB. The green lines on the figures indicate the side lobe level.

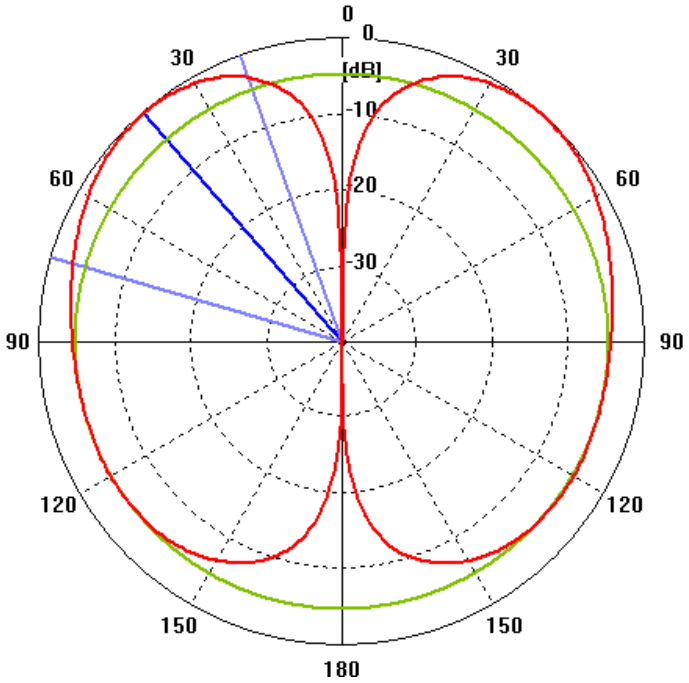

Figure 4-22 Far field radiation pattern in the y-z plane at 1.9 GHz

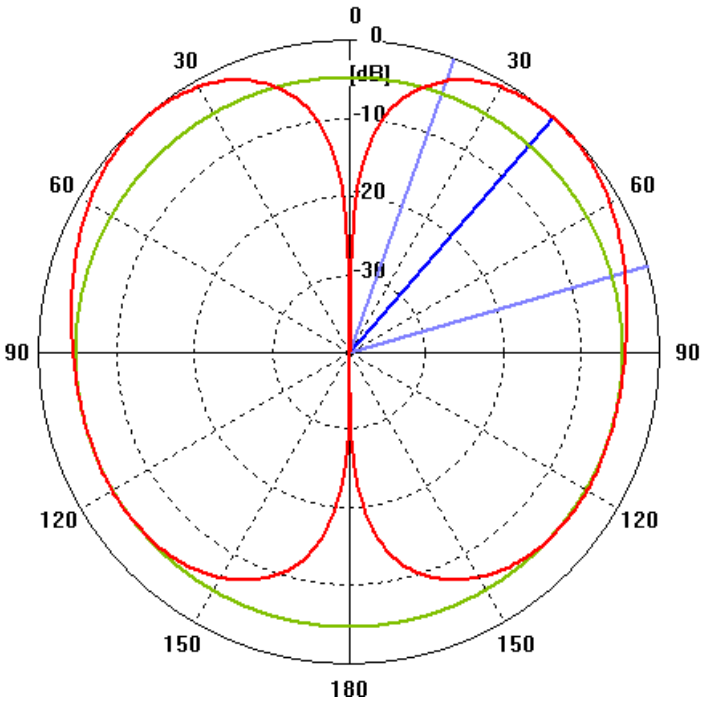

Figure 4-23 Far field radiation pattern in the x-y plane at 1.9 GHz

Far field radiation pattern for axial polarization at 2.59 GHz in x-z plane is presented in Figure 4-24. Maximum directivity in aforementioned plane is 3.1 dB while -1.5 dB is the minimum which happens on top of each patch. Highest cross polarization component is -4.0 dB. This value is relatively higher than the value in 2.0 GHz; which is due to different current distributions at these two frequencies [41].

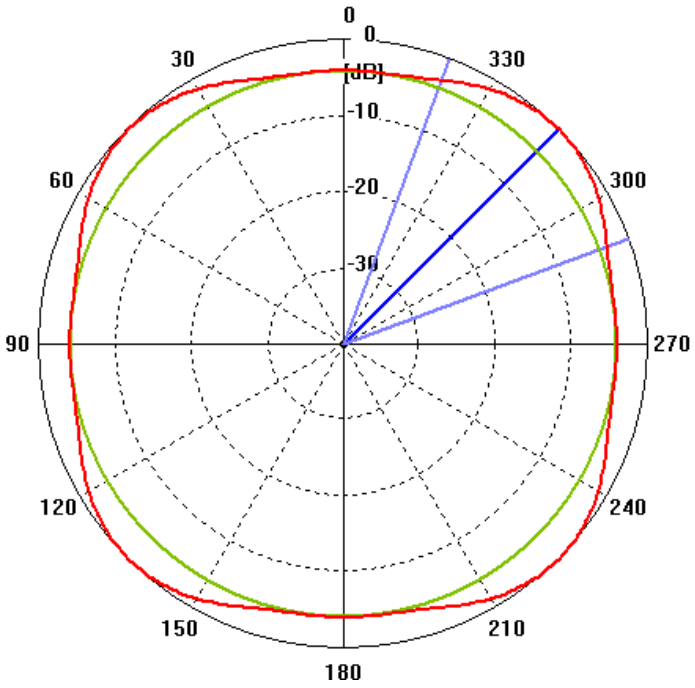

Figure 4-24 Far field radiation pattern in the x-z plane at 2.59 GHz

Far field radiation patterns at 2.59 GHz for axial polarization in y-z and x-y planes are plotted in Figure 4-25 and Figure 4-26 respectively. Highest directivity is 3.1 dB in these planes whereas maximum cross polarization is around -70 dB. Two nulls occur on y axis for both planes. Again the reason for asymmetry on the hemispheres is the slits. The green lines on the figures indicate the side lobe level.

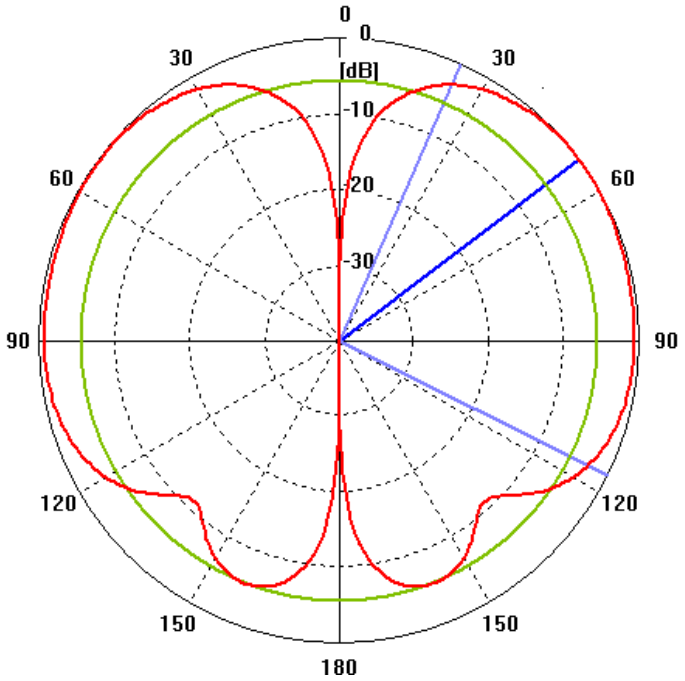

Figure 4-25 Far field radiation pattern in the y-z plane at 2.59 GHz

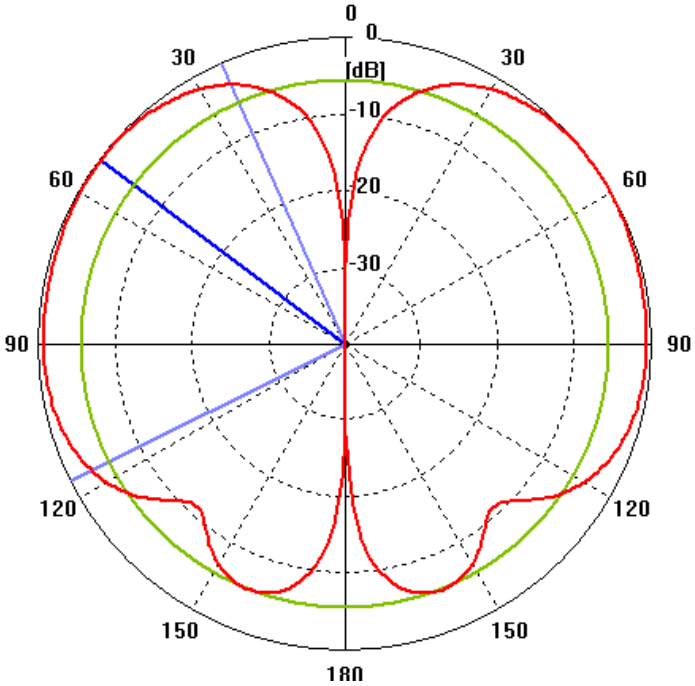

Figure 4-26 Far field radiation pattern in the x-y plane at 2.59 GHz

4.2.2 Eight Element Antenna Array Design

In this section a two dimensional array is designed having a higher directivity than the previous one. The design parameters are listed in Table 4-1, except R=130 mm and W_L = 2 mm in this case. Since axially polarized elements are positioned in axial direction, mutual coupling effects are stronger which change the input impedance of the antenna. That is the reason why W_L is decreased from 9 mm to 2 mm. The configuration of the array is illustrated in Figure 4-27. Circumferential element spacing, D_1 is 149 mm and axial spacing, D_2 is 40 mm. Antenna is axially polarized and excitation of the elements is with the same amplitude and phase.

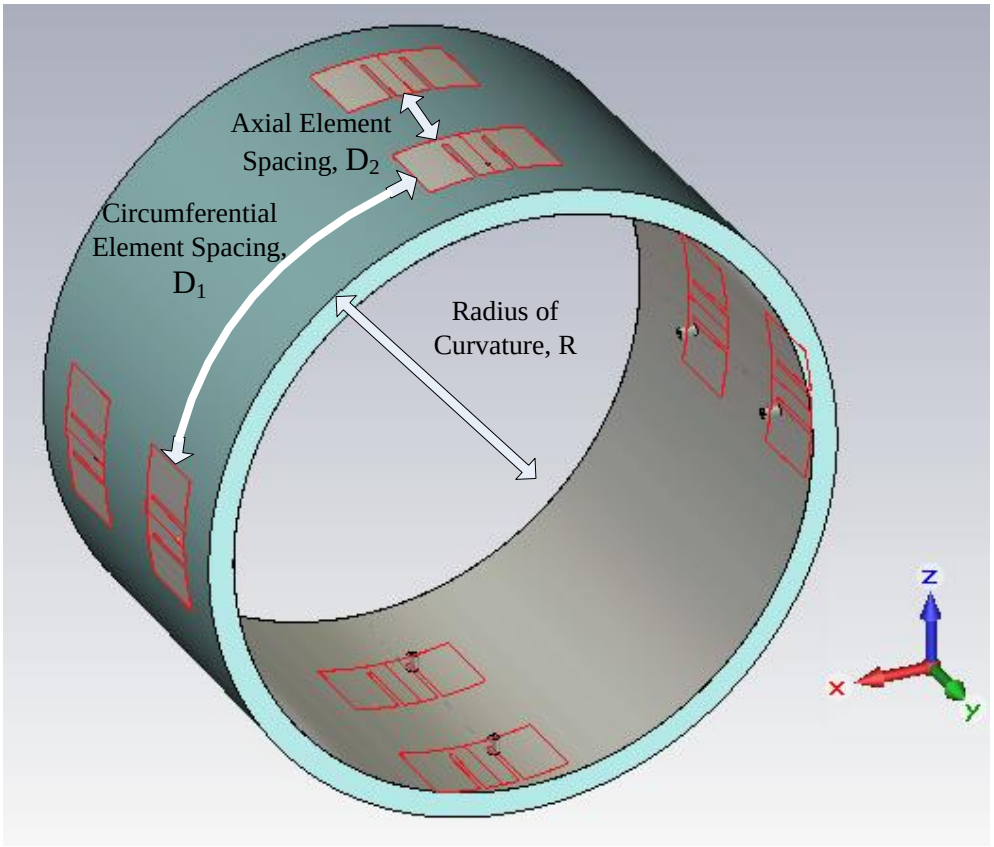

Figure 4-27 Geometry of the eight element array

Return loss for one element of the array is illustrated in Figure 4-28. Bandwidth of the antenna is 450 MHz, which is 20% of the center frequency.

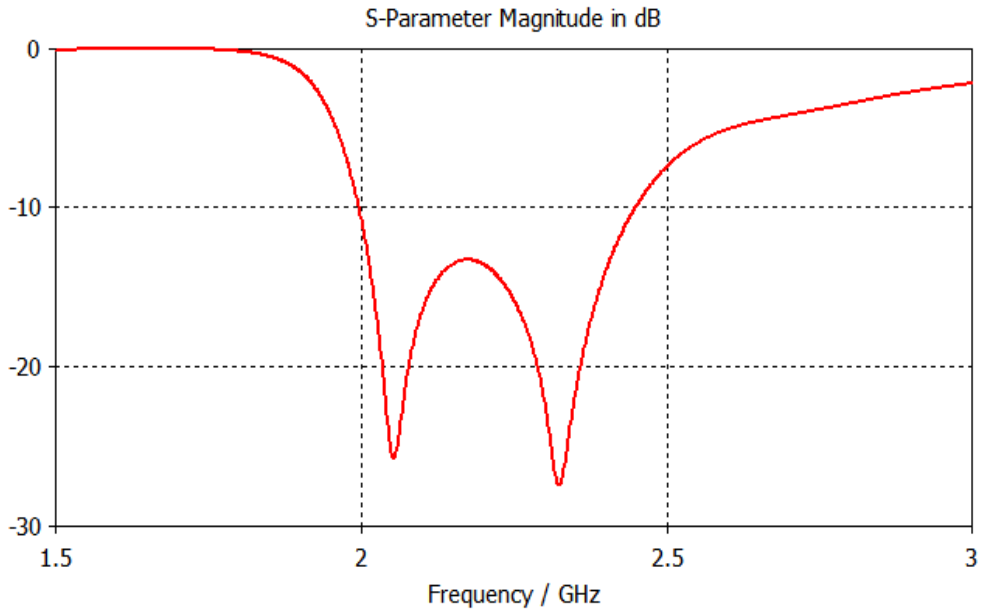

Figure 4-28 Return loss of the single element of eight element array

Figure 4-29 is the result of the far field radiation pattern for axial polarization at 2.0 GHz in the x-z plane. Maximum directivity is 5.4 dB while 0 dB is the minimum one. The higher directivity is due to the second element in axial direction and further increase can be achieved by using more elements in this direction. Cross polarization is not more than -15 dB in the aforementioned plane.

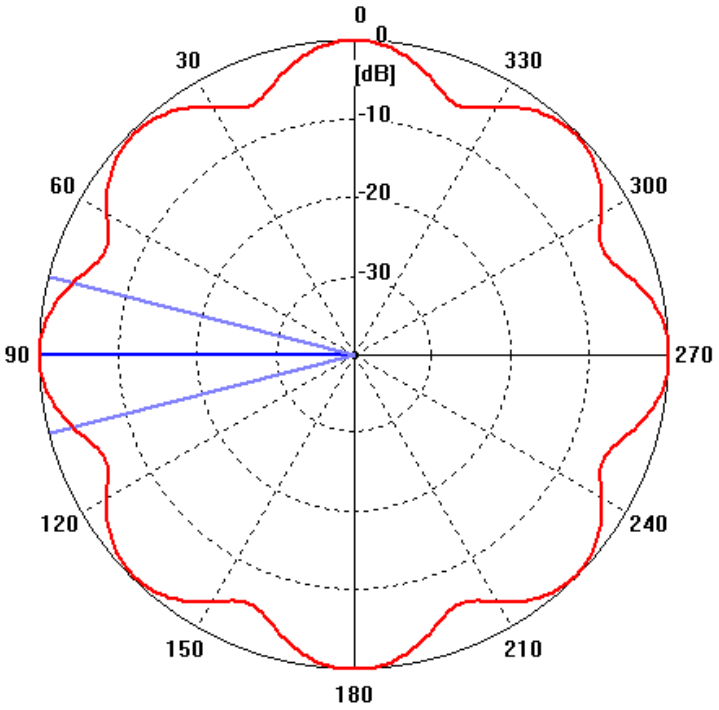

Figure 4-29 Far field radiation pattern in x-z plane at 2.0 GHz

Far field radiation pattern for axial polarization at 2.0 GHz in y-z and x-y planes are plotted in Figure 4-30 and Figure 4-31 respectively. In both planes, highest directivity is 5.4 dB and two nulls occur in y axis. Cross polarization is less than -60 dB in both planes. The green lines on the figures indicate the side lobe level.

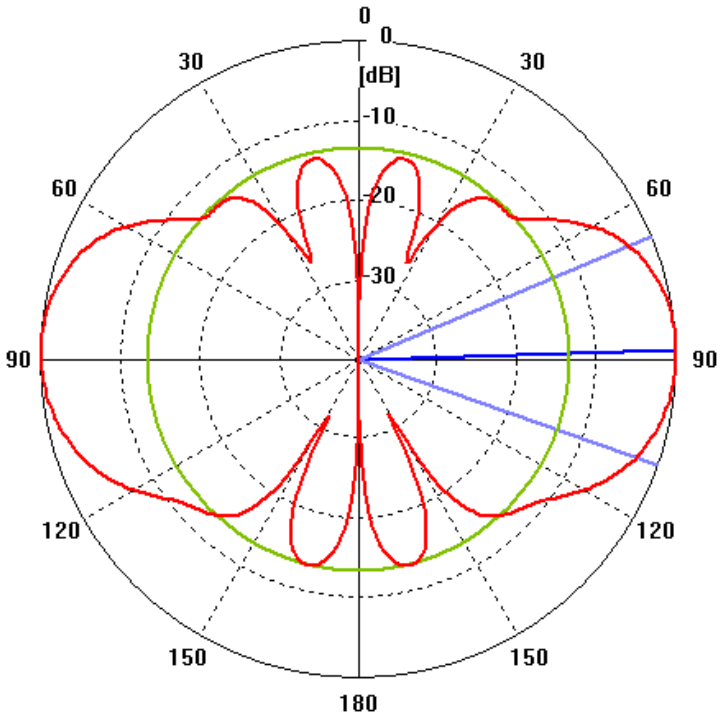

Figure 4-30 Far field radiation pattern in y-z plane at 2.0 GHz

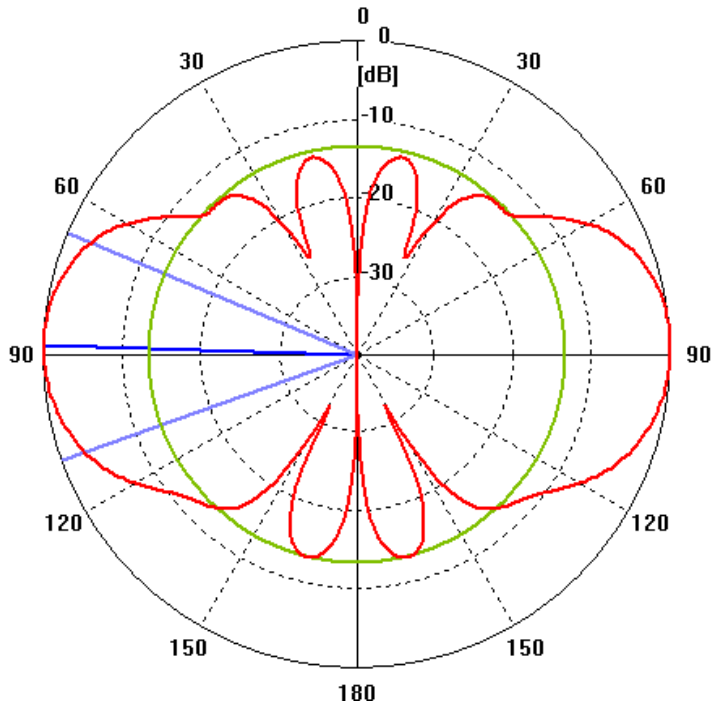

Figure 4-31 Far field radiation pattern in x-y plane at 2.0 GHz

Far field radiation pattern for axial polarization at 2.45 GHz in the x-z plane is illustrated in Figure 4-32. The antenna has an omnidirectional radiation pattern in this plane with 6.2 dB maximum and -2.5 dB minimum directivities. Maximum cross polarization is around -6 dB.

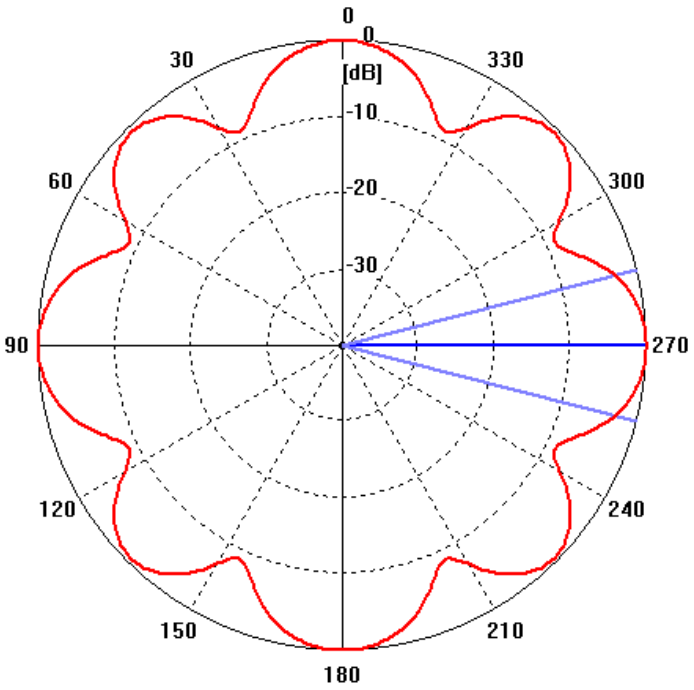

Figure 4-32 Far field radiation pattern in x-z plane at 2.45 GHz

Far field radiation patterns for axial polarization at 2.45 GHz in the y-z and x-y planes are shown in Figure 4-33 and Figure 4-34 respectively. For both figures, two nulls occur in y axis and maximum directivity is 6.2 dB. The highest cross-polarization component in both planes is less than -60 dB. The green lines on the figures indicate the side lobe level.

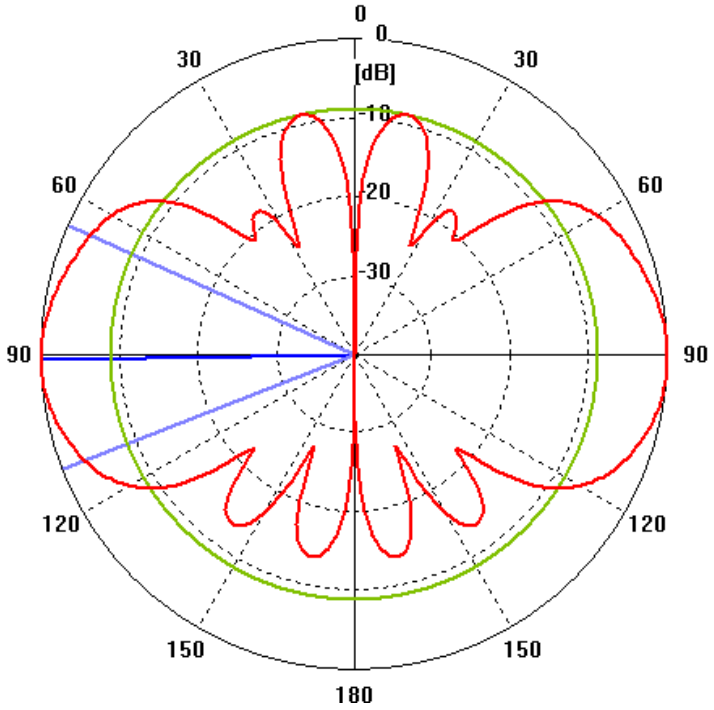

Figure 4-33 Far field radiation pattern in y-z plane at 2.45 GHz

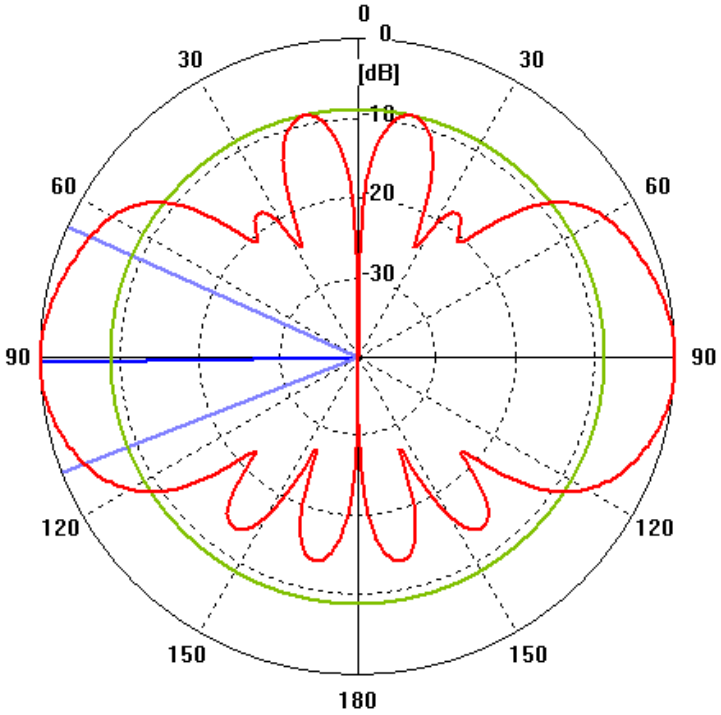

Figure 4-34 Far field radiation pattern in x-y plane at 2.45 GHz

4.3 Verification of the Simulation Method

In order to verify the simulation tool, the fabricated compact broadband antenna in [33] is simulated in CST. The geometry details of the antenna are illustrated in Figure 4-35, Figure 4-36 and Table 4-7. The substrate is foam; the inner and outer diameters of the 50 ohm coaxial probe are 1.27 mm and 4.1 mm, respectively.

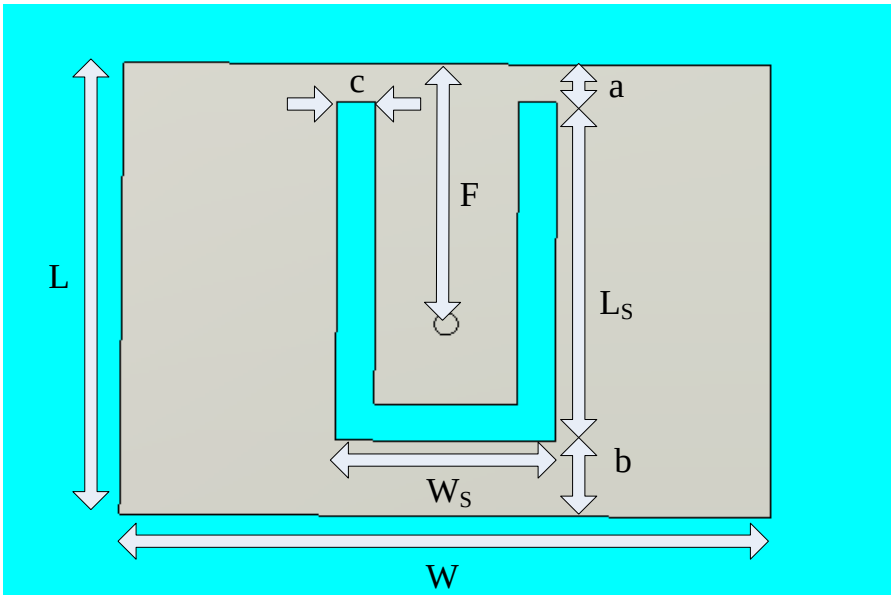

Figure 4-35 Geometry of the compact broadband antenna – top view

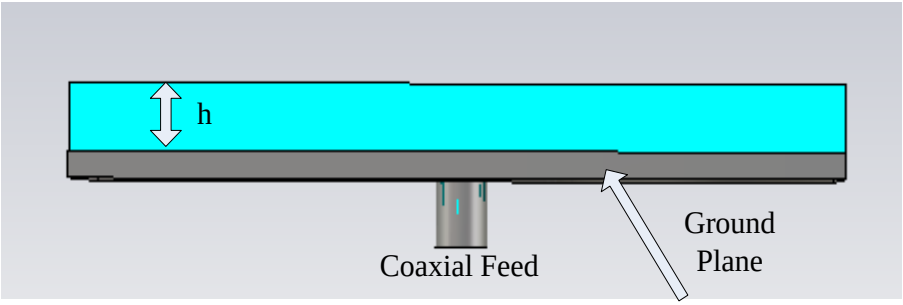

Figure 4-36 Geometry of the compact broadband antenna – side view

Table 4-7 Dimensions of the compact broadband antenna in milimeters

W	L	F	W_S	L_S	a	b	c	h
35.5	26.0	15.0	12.0	19.5	2.2	4.3	2.1	5.0

Figure 4-37 provides the fabrication and CST simulation results for VSWR of the antenna in [33]. It is clear from both figures that simulated VSWR in CST is nearly the same with the measured VSWR result. Some very small differences may be due to fabrication tolerances and numerical errors of the simulation tool.

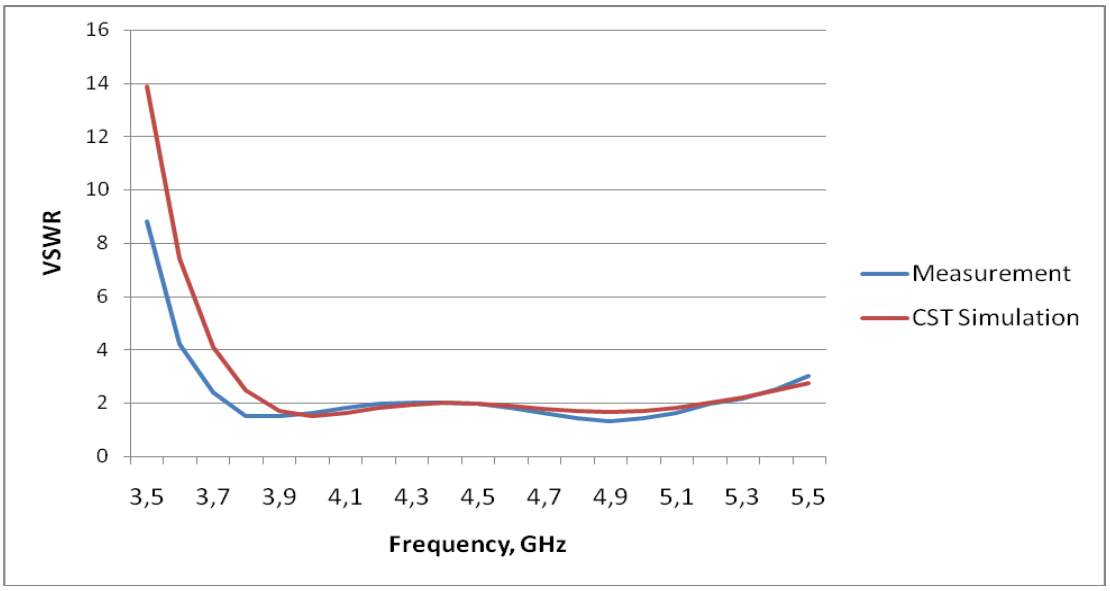

Figure 4-37 Experimental and CST simulation results for VSWR of the antenna in [33]

Measurement and CST simulation results for E- and H-plane radiation patterns of the antenna in [33] is given in Figure 4-38 and Figure 4-39. Similar results are obtained for main lobe in both planes. The difference between measurement and CST simulation results for back lobe radiation may be due to the thickness of the ground plane. Since this dimension is not given in [33], it is taken as 1mm.

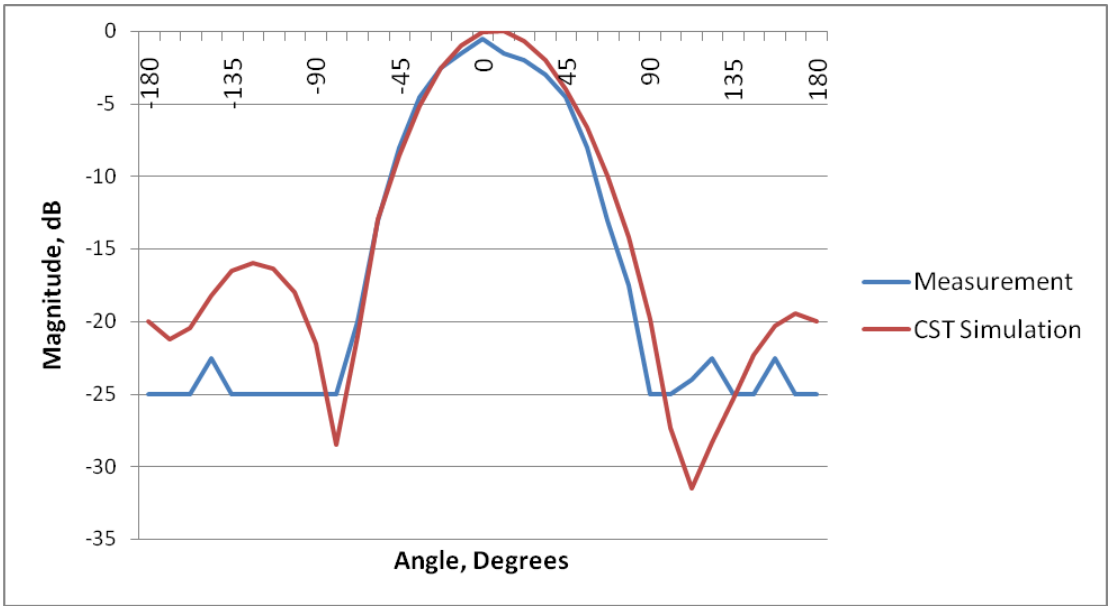

Figure 4-38 Experimental and CST simulation results for E-Plane Radiated Fields of the antenna in [33]

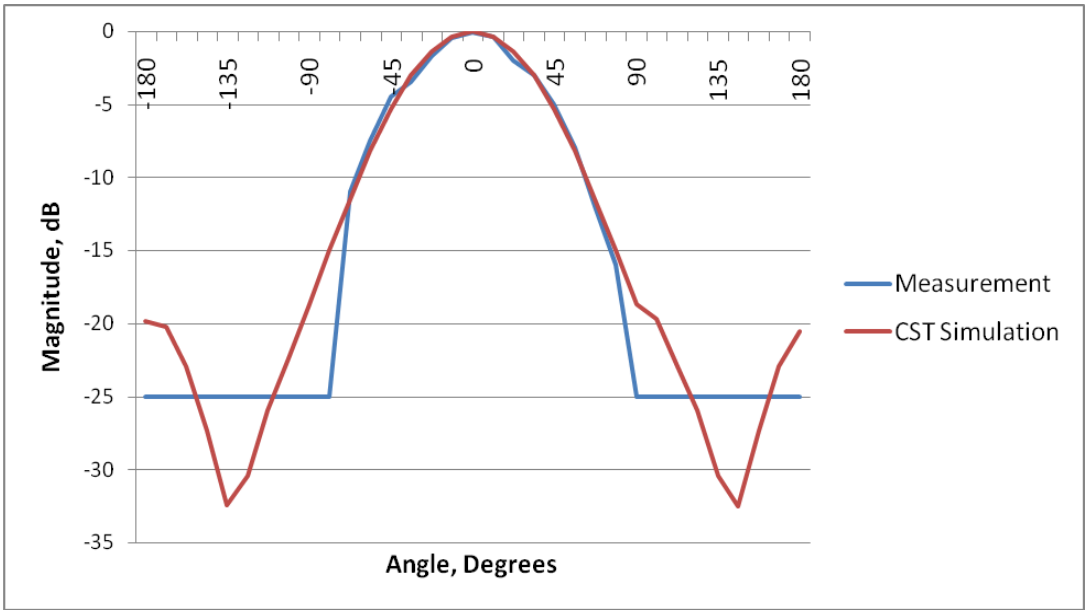

Figure 4-39 Experimental and CST simulation results for H-Plane Radiated Fields of the antenna in [33]

4.4 Conclusions

In this part of the thesis, parametric analysis of an E-shaped cylindrically conformal antenna is carried out initially. After that, two different conformal arrays are realized and simulation results regarding these arrays are presented. One of them has higher gain in the circumferential plane, and lower beam width in the other two planes, which may be required in some long range applications. Slit parameters and feed offset are crucial in determining the resonant frequency of the antenna. With proper adjustment of these parameters, bandwidths more than 30% can be achieved. Radiation pattern of the antenna is stable over the entire frequency range. To have a good impedance matching over a wide bandwidth, slit length to patch length ratio is found to be 0.7 to 0.85 and distance between outer edges of the slits is about 0.27 times patch width [40]. These dimensions can change but they are still good starting point for initializing the design. Dual frequency of operation is also possible with E-shaped antenna. At the end of this chapter, a fabricated compact broadband antenna is simulated in CST to verify the simulation method.

CHAPTER 5

CONCLUSIONS AND FUTURE WORK

In this thesis proximity coupled and E-shaped cylindrically conformal microstrip antennas are studied. Parametric analysis of these structures is performed to observe the effect of design parameters on return loss and radiated fields of the antenna. Two cylindrical arrays are designed for both antenna types and simulation results are presented. CST MICROWAVE STUDIO® is used to perform the electromagnetic simulations.

Proximity coupled microstrip antenna element is designed with flexible Arlon IsoClad 933 substrate having 3.15mm thickness. It is shown that resonant frequency does not change with radius of curvature for axial polarization. Bandwidth of a cylindrically conformal antenna is found to be higher than the planar case of the same antenna. In addition, back radiated field of the antenna increases when radius of curvature decreases. By using the proximity coupled antenna element, two different cylindrical array configurations are realized. It is observed that omnidirectional radiation is accomplished by wrapping a microstrip antenna array around a cylinder.

Design parameters of E-shaped conformal microstrip antenna element are investigated and valuable design information is given. With a very compact structure, bandwidth more than 30% is obtained. Very small changes are observed on the return loss characteristics of this wideband antenna as radius

of curvature changes. Additionally, an omnidirectional radiation with a higher gain is obtained by placing more than one element in axial direction. In the last step, a fabricated antenna is simulated in CST and acceptable agreement is observed with the simulation and fabrication results.

For future work, an enclosing radome could be used to protect the antenna from environmental effects. Since the overall thickness increases, resonant frequency and bandwidth will change depending on the material type of the radome. The radome also needs to be flexible in order to allow bending and should be glued or clinched to the antenna not to allow an air gap between the radome and the antenna.

Another future work is feeding the array elements with different amplitudes or phases. By this way the pattern can be directed in any desired direction or the pattern has a null in a direction where an electronic warfare system is located. Compact wideband microstrip antennas are of great interest in recent years and finding design equations of these antennas would be a great research subject.

REFERENCES

[1] G. A. Deschamps, "Microstrip Microwave Antennas," *Proc. 3rd USAF Symposium on Antennas,* 1953

[2] R. E. Munson, "Conformal Microstrip Antennas and Microstrip Phased Arrays," *IEEE Trans. on Antennas and Propagation,* Vol. AP-22, 1974, pp. 74-78

[3] J. Q. Howell, "Microstip Antennas," *IEEE APS Int Symp. Digest*, 1972, pp.177-180

[4] R. Garg, P. Bhartia, I. Bahl and A. Ittipiboon, "Microstrip Antenna Design Handbook," Artech House, 2001

[5] G. Kumar and K. P. Ray, "Broadband Microstrip Antennas," Artech House, 2003

[6] A.K. Shrivastavl, A. Das and S. K. Das, "Wide Band Omni Directional Radiating Array for Cylindrical Body" *Proceedings of International Conference on Electromagnetic Interference and Compatibility (INCEMIC)*, 2003, pp. 359-360

[7] C. A. Balanis, "Antenna Theory Analysis and Design Second Edition," John Wiley & Sons, United States of America, 1997

[8] E. O. Hammerstad, "Equations for Microstrip Circuit Design," *Microwave Conference*, 1975, pp. 268-272

[9] M. V. Schneider, "Microstrip dispersion," *in Proc. IEEE*, Vol. 60, Jan. 1972, pp. 144-146

[10] Y. T. Lo, D. Solomon, and W. F. Richards, "Theory and Experiment on Microstrip antennas," *IEEE Trans. Antennas and Propagation*, Vol. AP-27. No. 2, March 1979, pp. 137-145

[11] J. R. James and P. S. Hall, "Handbook of Microstrip Antennas," Peter Peregrinus Ltd., United Kingdom, 1989

[12] R. C. Booton, "Computational Methods for Electromagnetics and Microwaves," John Wiley & Sons, United States of America, 1992

[13] T. Weiland, "A Discretization Method for the Solution of Maxwell's Equations for Six-component Fields" *Electronics and Communication AEU*, Vol. 31, No. 3, March 1977, pp. 116-120

[14] L. Josefsson and P. Persson "Conformal Array Antenna Theory and Design," IEEE Press, 2006

[15] B. R. Piper and M. E. Bialkowski, "Electromagnetic Modeling of Conformal Wideband and Multi-band Patch Antennas by Bridging a Solid-Object Modeler with MoM Software," *IEEE Antennas and Propagation Magazine,* Vol. 46, No. 5, October 2004, pp. 42-52

[16] K. M. Luk, K. F. Lee, J. S. Dahele, "Analysis of the Cylindrical-rectangular Patch Antenna," *IEEE Trans. Antennas and Propagation,* Vol. 37, No. 2, February 1989, pp. 143-147

[17] C. M. Krowne," Cylindrical-Rectangular Microstrip Antenna," *IEEE Trans. on Antennas and Propagation,* Vol. AP-31, 1983, pp. 74-78

[18] Z. Sipus, P-S. Kildal, R. Leijon, and M. Johansson, "An Algorithm for Calculating Green's Function of Planar, Cylindrical and Spherical Multilayer Structures," *ACES Journal*, Vol.13, No. 3, 1998, pp. 243-254

[19] V. B Ertürk, and R. G. Rojas, "Efficient Analysis of Input Impedance and Mutual Coupling of Microstrip Antennas Mounted on Large Coated Cylinders," *IEEE Trans. on Antennas and Propagation,* Vol. 51, No. 4, April 2003, pp. 739-749

[20] A. Sabban "A New Broadband Stacked Two Layer Microstrip Antenna," *IEEE Antennas and Propagation Society International Symposium*, June 1983, pp. 63-66

[21] R. Q. Lee, K.F. Lee, and J. Bobinchak, "Characteristics of a Two Layer Electromagnetically Coupled Rectangular Patch Antenna," *Electronic Letters*, Vol. 23, No. 20, September 1987, pp. 1070-1072

[22] G. Splitt, and M. Davidovitz, "Guidelines for Design of Electromagnetically Coupled Microstrip Patch Antennas on Two-Layer Substrates," *IEEE Trans. on Antennas and Propagation*, Vol. AP-38, No. 7, 1990, pp. 1136-1140

[23] H. G. Oltman, and D. A. Huebner, "Electromagnetically Coupled Microstrip Dipoles," *IEEE Trans. on Antennas and Propagation,* Vol. AP-29, No. 7, 1981, pp. 151-157

[24] P. B. Katehi, and N. G. Alexopoulos, "On the modeling of Electromagnetically Coupled Microstrip Antennas-The Printed Strip Dipole," *IEEE Trans. on Antennas and Propagation*, Vol. AP-32, No. 11, 1984, pp. 1179-1186

[25] M. Davidovitz, and Y. T. LO, "Rigorous Analysis of a Circular Patch Antenna Excited by a Microstrip Transmission Line," *IEEE Trans. on Antennas and Propagation,* Vol. 37, No. 8, August 1989, pp. 949-958

[26] B. Belentepe, "Modeling and Design of Electromagnetically Coupled Microstrip-Patch Antennas and Antenna Arrays," *IEEE Trans. on Antennas and Propagation,* Vol. 37, No. 1, February 1995, pp. 31-39

[27] D. M. Pozar "Microstrip Antenna Aperture Coupled to a Microstrip Line," *Electronics Letters,* Vol. 21, No. 2, 1985, pp. 49-50

[28] D. M. Pozar, "A Reciprocity Method of Analysis for Printed Slot-Coupled Microstrip Antennas," *IEEE Trans. on Antennas and Propagation,* Vol. AP-34, 1986, pp. 1439-1445

[29] P. L. Sullivan, and D.H. Schaubert, "Analysis of an Aperture-Coupled Microstrip Antenna," *IEEE Trans. on Antennas and Propagation,* Vol. AP-34, No. 8, 1986, pp. 977-984

[30] M. Himdi, J. P. Daniel, and C. Terret, "Transmission Line Analysis of Aperture Coupled Microstrip Antennas," *Electronics Letters,* Vol. 25, 1989, pp. 1229-1230

[31] M. Himdi, J.P. Daniel, and C. Terret, "Analysis of an Aperture Coupled Microstrip Antenna Using Cavity Method," *Electronics Letters,* Vol. 25, No. 6, 1989, pp. 391-392

[32] T. Huynh, and K. F. Lee, "Single Layer Single Patch Wideband Microstrip Antenna," *Electronics Letters,* Vol. 31, No. 16, August 1995, pp. 1310-1312

[33] K. F. Lee, K. M. Luk, K. F. Tong, S. M. Shum, T. Huynh, and R. Q. Lee, "Experimental and Simulation Studies of the Coaxially Fed U-Slot Rectangular Patch Antenna," *IEE Proc. Microwaves, Antennas Propagation,* Vol. 144, No. 5, 1997, pp. 354–358.

[34] M. Clenet and, L.Shafai, "Multiple Resonances and Polarization of U-Slot Patch Antenna," *Electronics Letters,* Vol. 35, No. 2, January 1999, pp. 101-103

[35] K. F. Tong, K. M Luk, K. F. Lee, and R. Q. Lee, "A Broad-Band U-Slot Rectangular Patch Antenna on a Microwave Substrate" *IEEE Trans. on Antennas and Propagation,* Vol. 48, No. 6, June 2000, pp. 954-960

[36] Y. L. Chow, Z. N. Chen, K. F. Lee, and K. M. Luk, "A Design Theory on Broadband Patch Antennas with Slot", *IEEE Antennas and Propagation Society International Symposium,* Vol. 2, June 1998, pp. 1124-1127

[37] R. Bhalla, and L. Shafai, Resonance Behavior of Single U-Slot and Dual U-Slot Antenna, *Antennas and Propagation Society International Symposium,* Vol. 2, 2001, pp. 700-703

[38] S. Weigand, C. H. Huff. K. H. Pan and J. T. Bernhard "Analysis and Design of Broad-Band Single-Layer Rectangular U-Slot Microstrip Patch Antennas," *IEEE Trans. on Antennas and Propagation,* Vol. 51, No. 3, March 2003, pp. 457-469

[39] K. L. Wong and W. H. Hsu, "A broadband rectangular patch antenna with wide slits," *Antennas and Propagation Society International Symposium,* Vol. 3, 2000, pp. 1414-1417

[40] K. L. Wong and W. H. Hsu, "A broad-Band Rectangular Patch Antenna With a Pair of Wide Slits," *IEEE Trans. on Antennas and Propagation*, Vol. 49, No. 9, Sept. 2001, pp. 1345-1347

[41] F. Yang, X. X. Zhang, X. Ye, and Y. Rahmat-Samii, "Wide-band E-shaped patch antennas for wireless communications," *IEEE Trans. on Antennas and Propagation*, Vol. 49, No. 7, July 2001, pp. 1094-1100

[42] A. A. Lotfi Neyestanak, F. Hojjat Kashani, and K. Barkeshli, "E-Shaped Patch Antenna Design Based on Genetic Algorithm Using Decision Fuzzy Rules," *Iranian Journal Of Electrical And Computer Engineering*, Vol. 4, No. 1, Winter-Spring 2005, pp. 18-24

[43] CST Microwave STUDIO®, User Manual, CST GmbH.